Modern Applied Science; Vol. 12, No. 4; 2018
ISSN 1913-1844 E-ISSN 1913-1852
Published by Canadian Center of Science and Education

Hydrogen Sulfide Corrosion of Carbon and Stainless Steel Alloys in Mixtures of Renewable Fuel Sources under Co-Processing Conditions

András Gergely[1], Péter Szabó[2], Antal Krójer[3], Bence Nagy[4] & Tamás Kristóf[1]

[1] Department of Physical Chemistry, Institute of Chemistry, University of Pannonia, Egyetem u. 10., Veszprém, 8200, Hungary

[2] Department of General and Inorganic Chemistry, Institute of Chemistry, University of Pannonia, Egyetem u. 10., Veszprém, 8200, Hungary

[3] Department of Inspection and Maintenance, Mol Nyrt., Olajmunkás u. 2., Százhalombatta, 2443, Hungary

[4] Refining Research and Innovation, Mol Nyrt., Olajmunkás u. 2., Százhalombatta, 2443, Hungary

Correspondence: András Gergely, Department of Physical Chemistry, Institute of Chemistry, University of Pannonia, Egyetem u. 10., Veszprém, 8200, Hungary Tel: 36-88-624-000-6044, 36-70-272-1994. E-mail: gergelyandras432@gmail.com

Received: December 29, 2018 Accepted: January 11, 2018 Online Published: March 31, 2018

doi:10.5539/mas.v12n4p227 URL: https://doi.org/10.5539/mas.v12n4p227

The research is financed by the GINOP-2.3.2-15-2016-00053 project with title of "Development of engine fuels with high hydrogen content in their molecular structures (contribution to sustainable mobility)".

Abstract

Corrosion rates of steel alloys were investigated in gas oil and its mixture with waste cooking oil and animal waste lard over 1, 3, 7 and 21 days under desulfurizing condition. Co-processing conditions were attempted to simulate by batch-reactor experiment at temperatures between 200 and 300°C and pressures between 20 and 90 bar in the presence of 2 volume% hydrogen sulfide. Integral and differential corrosion rates were defined by weight losses. Intense sulfide corrosion of carbon steels was less impacted by the biomass sources. Thinner scales in gas oil was probably due to frequent cohesive failure, whereas thicker layers in biomass mixtures were allowed to form to afford limited physical protection. The high corrosion rate of low alloy steel with temperature over time is related to inefficient protection by the metal sulfide scales. Greater activation energy and enthalpy balance in the formation of activated complex is expected to reflect in thick cohesive scales. Loose layers and the less unfavorable entropy balance in the transition state did not lead to valuable barrier protection. High sulfide corrosion resistance of stainless steels is in chemical in nature markedly impacted by the biomass fuel sources and contributed especially by the acidic species. Corrosion rates increased with temperature by magnitude similar to those of carbon steels, which probably owes to the less unfavorable entropy and free energy balance between the initial and transition states of the reactants.

Keywords: hydrogen sulfide corrosion, engineering steel alloys, renewable biofuel sources, spalling, porous & compact sulfide scales

1. Introduction

1.1 Introduction of the Problem

Biomass fuel sources like vegetable oils and their waste products besides animal waste lard (AWL) are appropriate renewable feedstock for partial substitution of mineral oils in production of biofuels. Composition of vegetable oils rich in natural triacylglycerols is similar to AWL. Biodiesel production is based on trans-esterification or catalytic hydrocracking. Technological parameters of the latter mean temperatures of 320–430°C and pressures of 3.5–5.5 MPa with relative content of the biomass of around 5.5% (Mikulec J, et al., 2010). High iso-paraffin content is obtained by catalytic hydrogenation of AWL (Hancsók J, et al., 2011). Some vegetable oils like tall oil with high free-fatty acid content (Craig WK & Soveran DW, 1991; Stumborg M, et al., 1996; Monnier J, et al., 1998; Klass DL, 2004; Knothe G, et al., 2005) is similar to AWL. Heteroatom contents of all fuel sources must be

decreased to circumvent environmental pollution and higher degree of corrosion risks in subsequent applications. In the aspects of safety and profitability, the one should consider corrosion of metallic structures of the existing petroleum refineries caused by renewable biomass fuel sources.

Raw plant oils, waste cooking oil (WCO) and AWL assessed under co-processing conditions caused negligible metal leaching (Melero JA, 2010). Interestingly, the free fatty acids (FFAs) of plant and AWL sources did not cause higher corrosion of carbon steel (CS, ASTM A 293 Gr C). Nonetheless, corrosivity of AWL depended on quantity and composition of the FFAs (Topolnitskij P, 2007). Stable passive oxide layers on surface of the 304L (1.4307) stainless steel (SS) and aluminum alloys is reason to their acceptable corrosion resistance. Corrosion kinetics of low and moderate allow steels caused by naphthenic acids and hydrogen sulfide were investigated at 270ºC in oils with naphthenic acid and sulfur contents of up to 1.0 wt.% (Qu DR, 2006). In the presence of naphthenic acids, low alloy (LA) and CSs indicated nearly the same corrosion rates but the former showed higher rates above 230ºC. When dimethyl disulfide was used, then corrosion rates obeyed parabolic kinetic law in time and film growth was faster on CS than on LAS. In fuel sources having naphthenic acids and dimethyl disulfide, LAS showed lower corrosion rates than CS. Scale formation in sulfide corrosion proved to be rate governing. Thus, different corrosion resistance of steels is also expressed in structure of the scales. Chromium sulfide layers behave as pseudo-passive films on high allow steels, in contrast with the scales composed of pyrrhotite (Fe_7S_8) and troilite (FeS) on CSs. Nevertheless, response of the pseudo-passivating films to the presence of biomass sources in the liquid phase has not been substantially explored so it is yet to be discovered. In addition, besides the numerous results on low temperature corrosion of automotive parts by biofuel sources, there is little known on corrosion rates of engineering steel alloys in renewable biofuel sources under HDS co-processing conditions.

Therefore, this work investigates hydrogen sulfide corrosion rates of two CSs (1.0425 and St35.8), a LAS (1.7335) and a sort of SS (1.4541) in the presence of gas oil and addition of renewable biomass fuel sources. The reason for selection of these steel samples, carbon and low alloy steels are used in pipe systems as heat-resistant materials, and stainless steels are usually utilized in absorbers, strippers and overlays in reactors. The effect of experimental variables is analyzed on the rate and activation of hydrogen sulfide corrosion of steel alloys.

2. Method

2.1 Batch Reactor Experiments

In advance of hydro-processing reactors, unsaturated and saturated FFAs are responsible to corrosion failure, after pipeline system and absorbers are impacted by hydrogen sulfide. To simulate process conditions, biomass sources were under conditions similar to HDS plants. Laboratory experiments were performed in two reactors having inner volumes of 4 and 2 liters. Temperature was measured through SS casings fixed with Pt100 resistive-thermometers and adjusted with controllers in ±5ºC. Heating and cooling were carried out as rapidly as possible in all experiments. During cooling phases, when temperature of 200ºC reached or the pressure dropped to 70% of the one maintained at the experiment, was regarded as end of the experiments.

Steel coupons of standard size, i.e., 32 mm outer and 10.5 inner diameters with thickness of 2 mm were first engraved with numbers for identification purposes. Rust and stain spots were removed by polishing with water wet silicon carbide papers (#400 and #600 in series). Then specimens were ultra-sonicated twice for 5 min in isopropanol and once in acetone. After drying, mass of the coupons was measured with an analytical balance. Composition of steel alloys are summarized in Table A1. Coupons were assembled on glass rods with spacers, inserted into glass tubes filled with gas oil and the biomass sources in 10 wt.%. Gas oil (GO), waste cooking oil (WCO) and AWL were supplied by the MOL Nyrt., which composition are given in Appendix (Table A2. and A3.). The most corrosive type AWL (with high FFA content) was used for the tests. The 4 times of 5 coupons of each alloy were placed in glass tubes which were fitted with inner and outer glass caps. Proportion of the gas and fluid phases was set close to each other in both reactors. Corrosion rates were defined over time periods besides assessing standard deviation of experiments of one autoclave test. Bottled hydrogen gas (2.5ip) with the purity of 99.5% was used as received from Messer Hungarogáz Kft., Hungary. The van der Walls constant of 2.67×10^{-5} m^3 mol^{-1} roughly equal to the 2nd Virial coefficient was used calculate hydrogen fugacity at temperatures of the experiments. By reactor fill-ups, gas pressure was measured both by pressure reducers (200/200 and 200/60, supplied by Messer Hungarogáz Kft., Hungary) and pressure gauges (calibrated before and after experiments) fixed in reactor heads. The hydrogen sulfide was in situ produced from stoichiometric quantity of elemental sulfur with an initial excess of ~10%. Before the series of autoclave tests, blind experiments were carried out to validate hydrogen sulfide content of the gas phase. Further details were given in earlier paper (Gergely A, 2016).

After the experiments, heavy oil and greasy residue were removed mechanically from the coupons then ultra-sonication in isopropanol was performed for three times (each for 10 minutes). Thickness of the sulfide scales on

the ferromagnetic CS and LAS alloys were measured with a Minitest 500 equipment (109-00-01 by Elektro-Physik, Köln, Germany). Average scale thickness was defined by data taken from 10 different areas on both sides of the coupons. Scales were removed by careful polishing, leaving intact metallic part of the steel coupons then their mass was measured to assess corrosion rates over time periods. Weight loss results were transferred into corrosion rates (mm year^{-1}) via the following formula:

$$\text{corrosion rate (mm year}^{-1}) = \frac{\Delta m * 365 * 1000}{\rho * A * t}, \quad (1)$$

where Δm: the measured weight loss (kg), ρ: density of the alloy (7870 kg m^{-3}), A: the reaction impacted geometric surface of the coupons ($1{,}702 \cdot 10^{-3}$ m^2) and t: time of exposure. The M molar weight of alloys used for calculations is given in kg mol^{-1} in the following: 5.58×10^{-2} for the 1.0425 (0.2% Ni and 1.1% Mn), 5.58×10^{-2} for the St35.8 (0.2% Ni, 0.6% Mn), 5.59×10^{-2} for the 1.7335 (1% Cr, 0.2% Ni, 0.5% Mo and 0.7% Mn), 5.54×10^{-2} for the 1.4541 (18% Cr, 9% Ni, 0.2% Mo and 2% Mn). Corrosion products on surface of the coupons were investigated along with local damages like pitting corrosion especially at grain boundaries.

2.2 X-ray Diffraction

Spalled sulfide layers were crushed and powdered, whereas loose scales were scrubbed and gathered. All were purified with two times of ultra-sonication in isopropanol for 10 minutes. XRD analysis was performed using a Philips PW 3710 powder diffractometer equipped with a PW 3020 vertical goniometer and curved graphite diffracted beam monochromator. The radiation of CuKα source was a broad-focus Cu tube operated at 50 kV and 40 mA. Measurements were carried out in continuous scan mode at a scanning rate of 0.02° s^{-1}. Data collection and evaluation were carried out with X'Pert Data Collector and X'PertHigh Score Plus software.

2.3 Scanning Electron Microscopy and Energy Dispersive Spectroscopy

Scales were removed from coupons, gathered and purified with two times of 10 min ultra-sonication in isopropanol. Morphology of the corroded coupons was performed with a scanning electron microscope (SEM, ESEM Philips XL31) in the secondary electron mode with an accelerating voltage of 20 kV, measuring and recording the images by back-scattered electrons. Elemental analysis was made with energy dispersive X-ray spectroscopy (EDX).

2.4 Optical Microscopy

A digital microscope from the VHX-2000 series (manufactured by Keyence) was used for visible light scanning of the surface of the corrosion tested coupons.

2.5 Micro-Raman spectroscopy

Purified corrosion products were probed five times at different spots. Raman measurements were performed at atmospheric pressure and gas composition. A Bruker Senterra Raman microscope was used with a source of green semiconductor-laser of 532 nm and maximum power of 10 mW. For the microscope, a 10x objective was used. Raman signals were collected with a charge-coupled device detector recording for 15 scans. A typical integration time for Raman spectra was 15 s on average with a resolution of 4 cm^{-1}.

3. Results

3.1 Batch reactor type Corrosion Experiments

3.1.1 Temperature Dependence

Temperature dependence of corrosion rates given in engineering relevant dimensions are summarized in Figures 1B (see Appendix). Corrosion rates of the 1.0425 CS were high and less dependent on temperature in GO. The alloy experienced lower corrosion rates in the biomass mixtures, with somewhat greater temperature dependence. Although corrosion rates were steep over the entire temperature range in WCO and AWL mixtures, the highest increase was obtained up to 250°C with pronounced impact to composition of the fluid phases. This is party connected to increasing rate of refining of the biomasses with temperature, leading to restrained degree of differences as integrity loss rates of the metals in batch experiments above 250°C (see the results of time dependence later). Even rate progression was obtained in AWL mixture despite the fact that CSs are more sensitive to sulfide corrosion and less distinctive to the biomasses.

Over medium long term, the St35.8 experienced greater corrosion rates in WCO and AWL mixtures at 200 and 225°C. Such dependence disappeared at 250°C and above, reaching maximum corrosion rates in neat raw GO and practically the same rates in the biomass mixtures (remained within variation of data) similarly to the 1.0425. As for corrosion resistivity of CSs, the St35.8 was seemingly thermally more activated susceptible for sulfide corrosion, than sensitive to the fluid phase over 504 hours at 250°C. The 1.7335 indicated the least varied corrosion

rates with the fluids, showing steady increase of sulfidation rates over temperate range. This indicates minimized effect of the organic phases nearly at all temperature over medium term since corrosion of the LAS was plausibly governed by the hydrogen sulfide and the rapidly developing sulfide scales (note results of the 24-hour experiment). Similarly, to the CSs, increasing temperature decreased impact of the fluid phases as mentionable effect of the biomasses was noticed at 250°C. Nevertheless, corrosion rates of the 1.7335 were the highest along CSs, pointing out its lower resistance to sulfide corrosion. Over medium long-time term, protective behavior and spalling failure of the scales might be assessed besides the proportion of sulfidic and acidic corrosion of the metals in the overall mass loss processes affected by the biomasses.

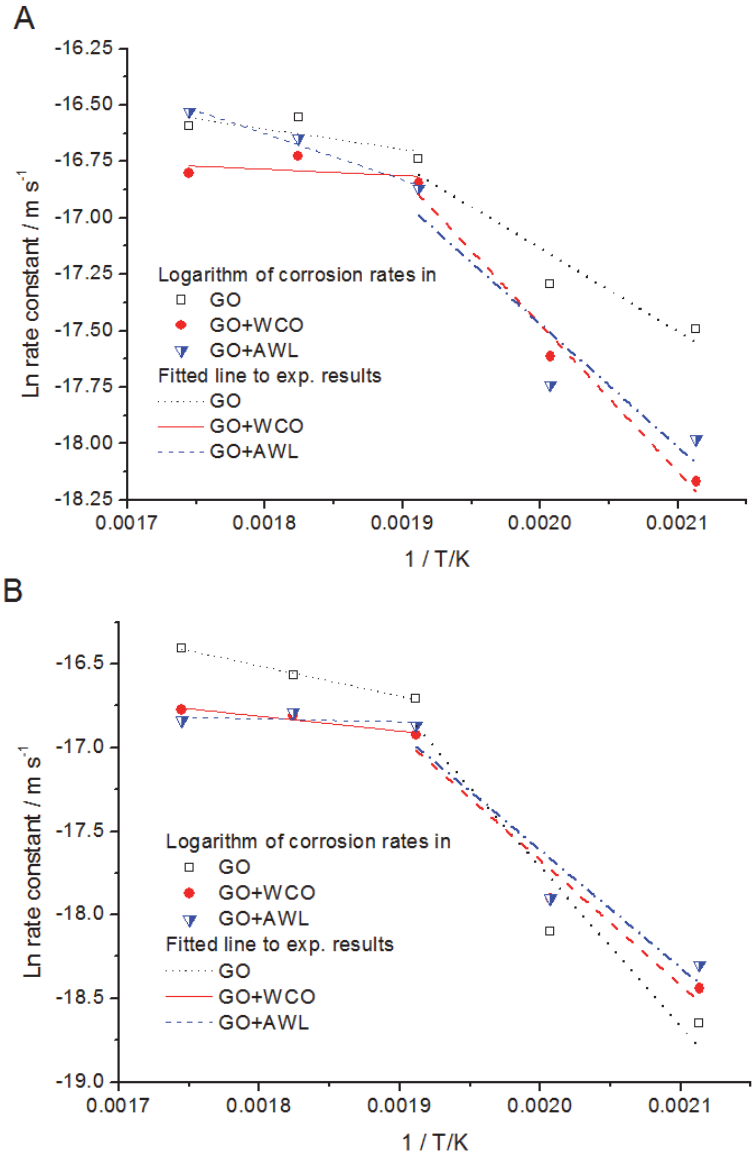

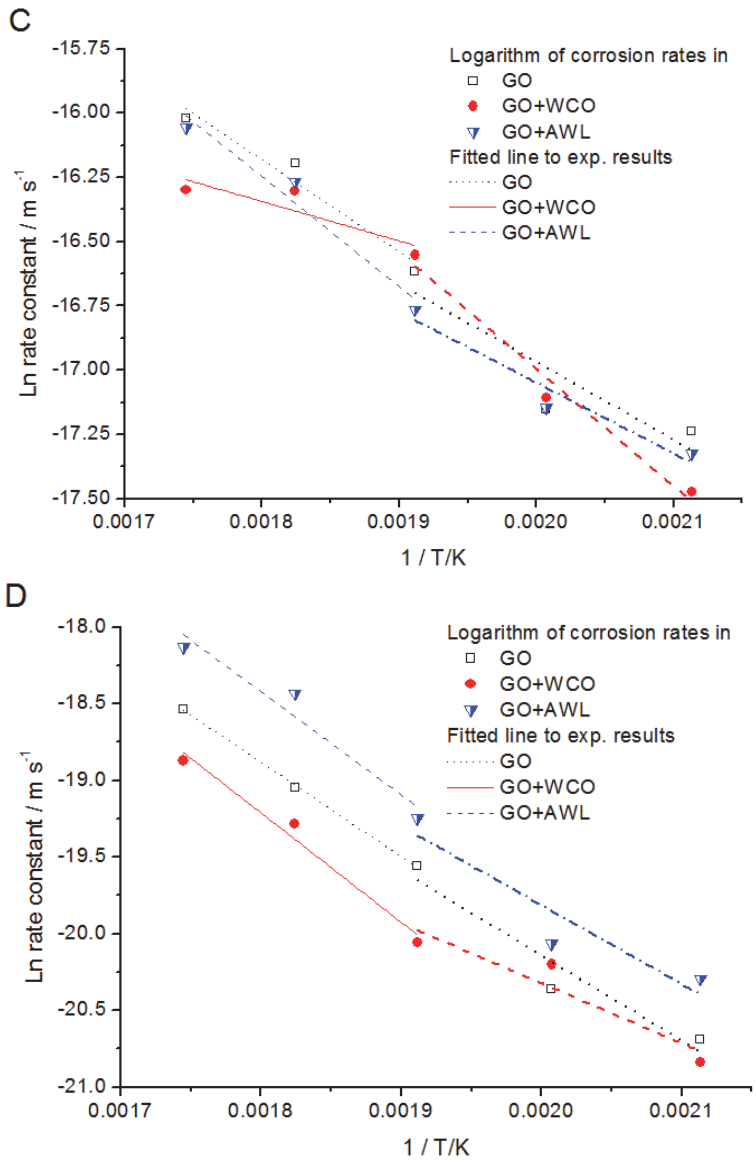

Figure 1. Logarithm of rate constants derived from integral corrosion rates (expressed in mol m^{-2} s^{-1}) over 504 hours in raw gas oil (GO) and its mixture either with waste cooking oil (WCO) or animal waste lard (AWL) tested at a pressure of 90 bar in the presence of 2 volume% hydrogen sulfide, fittings over temperature range between 200 and 300°C: A 1.0425, B St35.8, C 1.7335, D 1.4541

The 1.4541 SS indicated the lowest corrosion besides the highest variations depending on composition of the fluid phases over the entire temperature range. Although resistance of the steel almost levelled off up to 225°C, markedly increasing reaction rates were observed between 225 and 300°C. Increase of the integral corrosion rates was an order of magnitude quite similar to the ones obtained with the CSs. Impact of the fluid phases on resistance of the 1.4541 was pronounced over medium terms regardless of the temperature. Even though dense, compact and coherent scales developed on the surface (pronounced scaling tendency at higher temperature), the AWL mixture proved to be the most corrosive leading to much higher reaction rates at all temperature and minimizing protection role of the scales. The heavy biomass (10 wt.%) dependent corrosion is partly explained by composition of the AWL. As it is known, corrosion rates of the 18/8 type SS are expected around 30 µm $year^{-1}$ between 250 and 300°C in the presence of H_2S at 2 volume%. In our case, CSs showed much greater sulfidation rates than advised as acceptable of 0.25 mm $year^{-1}$ up to 390°C at a pressure of 34 Atm in the presence of 10 volume % of hydrogen sulfide (John RC, 1999).

Table 1. Apparent activation energy ($\Delta E^{\#}_r$ in kJ mol^{-1}), enthalpy ($\Delta H^{\#}_r$ in kJ mol^{-1}), Gibbs free energy ($\Delta G^{\#}_r$ in kJ mol^{-1}) and entropy ($\Delta S^{\#}_r$ in J mol^{-1} K^{-1}) derived from rate constants (m s^{-1}) based on logarithmic integral corrosion rates (mol m^{-2} s^{-1}) divided by concentration of the hydrogen sulfide, estimated by the Arrhenius and the Eyring–Polányi equations in the temperature ranges of 200-250°C and 250-300°C

Steels	$\Delta E^{\#}_r$ in raw GO		in GO+WCO		in GO+AWL	
	200-250°C	250-300°C	200-250°C	250-300°C	200-250°C	250-300°C
1.0425	31.0	7.3	54.6	2.2	45.9	16.9
St35.8	80.0	15.2	62.5	7.4	59.0	1.5
1.7335	25.6	29.7	38.1	12.6	23.1	35.4
1.4541	46.7	51.3	32.3	59.2	43.3	55.7
	$\Delta H^{\#}_r$ in GO		in GO+WCO		in GO+AWL	
1.0425	26.9	2.8	50.5	–2.4	41.8	12.4
St35.8	75.9	10.6	58.4	2.8	54.9	–3.1
1.7335	21.5	25.1	33.9	8.0	19.0	30.9
1.4541	42.5	46.7	28.2	54.6	39.2	51.2
	$\Delta S^{\#}_r$ in GO		in GO+WCO		in GO+AWL	
1.0425	–339	–383	–294	–393	–313	–366
St35.8	–247	–368	–281	–385	–288	–395
1.7335	–349	–339	–323	–371	–354	–329
1.4541	–333	–323	–361	–311	–337	–310
	$\Delta G^{\#}_r$ in GO		in GO+WCO		in GO+AWL	
1.0425	196	213	197	213	197	212
St35.8	199	213	198	214	198	213
1.7335	195	211	195	211	195	211
1.4541	209	224	208	225	207	221

Evaluation of experimental results based on the Arrhenius formalism (Arrhenius SA, 1889) are presented in Figures 1.A-D and apparent activation energies in the lower and upper temperature ranges are given in Table 1. Due to complexity of sulfide corrosion in fluids with biomasses, these results are regarded as high approximation. The 1.0425 and the St35.8 showed the most significant decreases in both activation energy and enthalpy between 250 and 300°C rather than in the range of 200-250°C. Variations depending on fuel mixtures were less remarkable. Activation to sulfide corrosion of the 1.0425 decreased only in WCO and increased in AWL mixture in comparison with that of experienced in GO. Kinetic hindrance of the St35.8 decreased more from the WCO to the one measured in AWL mixture. In the latter, the relevance of kinetic factors in accelerating corrosion rate of the St35.8 in matter of altered circumstances of reaching the transition state by the biomass components is evidenced. Over medium long-term, this is connected to decreasing resistance of the CSs. Catalytic effect of the sulfide scales to further corrosion is expected to occur at elevated temperature (besides greater scaling tendency at higher corrosion rates), which in cases seemed to be compensated by the biomasses to some extents. Comparable activation of CSs with the fuel mixtures at lower temperature means the lack of activation, some inhibition by the biomass components, contributing to restrained initiation of sulfide corrosion. Aside from decreasing activation to one third in WCO mixture, the 1.7335 indicated generally opposite trends, i.e., a somewhat greater activation barrier in GO and AWL mixture at upper temperatures compared to the lower one, whereas activation did not decrease in WCO mixture comparable to CSs with the increasing temperature. So, the higher activation in reaching the activated complex without faster corrosion rates with the increasing temperature is primarily connected to diffusion control in the solid state at the interface. Partly in accordance with the greater scaling tendency, some barrier effect of the sulfide scale should progressively evolve on the 1.7335 in GO and its AWL mixture and the protection efficiency might probably adversely have affected by some of the WCO components, e.g., citric, lactic and formic acids. This is in line with scale thickness measurement results (Table 2) performed after a 168 h test period at 275°C. Thin metal sulfide layers of ~13 μm formed in GO but scales of around three times thicker layers formed in WCO and AWL mixtures with greater thickness variation. In fact, thicker scales were composed of at least two layers of a metal sulfide and a deposited carbon layer, soot (see Raman spectroscopy results).

Given the highly uneven and incoherent microstructure of carbon films, only the former could provide some physical protection to the 1.7335 in WCO and AWL mixtures but none of the CSs showed similar results despite the much greater scale thicknesses in WCO and AWL mixtures compared to the ones grew in GO. The 1.4541 exhibited roughly the same and doubled activation control of sulfide corrosion in GO and its WCO mixture,

respectively. Around half of the activation barrier increase was found in AWL mixture with increasing temperature.

Table 2. Average thickness of sulfide scales (in μm) measured on the ferritic type carbon and low alloy steels tested for 168 hours at 275°C

	Thickness of the sulphide scales (μm) developed in		
Steel alloys	Gas oil	Gas oil + WCO	Gas oil + AWL
1.0425	10.5 ± 3.5	38.8 ± 7.6	31.2 ± 9.2
St35.8	15.8 ± 7.6	31.1 ± 8.7	33.2 ± 8.7
1.7335	13.1 ± 4.8	35.3 ± 7.8	27.1 ± 11.1

The almost negligible variation of thermal activation control in GO and AWL mixture at lower temperature suggests the same sort of reaction mechanism at least until formation of the transition complex took place. This picture changed when temperature was above 250°C then activation control became somewhat greater in fluids with the biomasses. This suggests slightly altered reaction mechanism in sulfide corrosion in the ways of greater proportion of corrosion activation of the alloying elements and mass transport through corrosion layers of the 1.4541, providing both physical and chemical protection at elevated temperature which was assisted by the biomass components. The former is kinetic and the latter thermodynamic in nature. Considering corrosion rates of the 1.4541 in GO and the biomasses along with degree of their progresses from lower to the upper temperatures, thermally activated acidic corrosion of the SS might become comparable to sulfidic processes of low temperature, obliterating any valuable physical protection by the scales. In fact, acidic corrosion of steels by the species being present in WCO and AWL such as acetic acid, iso-butyric acid, butyric acid and water, is expected to take over at elevated temperature during long times parallel with hydro-desulphurization. In another viewpoint, adsorption and dissolution of the metallic phase is probably hindered by the ductile coherent metal sulfides formed and metal-stabilized at higher temperature. In opposition, the almost doubled activation energy in WCO mixture is construed as pseudo-passivity, valuable protection by the metal sulfide films (see time dependence of corrosion rates). In other words, sulfide corrosion of the 1.4541 proved to be less disturbed kinetically by the biomasses when integrity loss rate with the related scaling tendency was low. This also points out that sulfide corrosion of the SS might proceed through complexes featuring the same kind and magnitude of activation control in GO as a function of temperature but greater scaling at higher temperature did not result in any considerable additional protection.

Table 3. Corrosion rates of steel alloys (in mm year^{-1}) over 504 hours immersed in raw and refined gas oils at 250°C at a pressure of 90 bar in the presence of 2 volume percent of hydrogen sulfide

Steel alloys	Raw gas oil	Refined gas oil
1.0425	0.50 ± 0.014	0.56 ± 0.017
St35.8	0.51 ± 0.010	0.61 ± 0.008
1.7335	0.56 ± 0.016	0.57 ± 0.020
1.4541	0.03 ± 0.001	0.03 ± 0.004

Refining of the raw GO itself should have not resulted in remarkable effect on corrosion rates as blind test results underscore it (Table 3). Difference between continuous and batch type experiments were probed the impact of hydrogenizing refining and compare corrosion rates in the presence and absence of sulfur containing species in the GO. Corrosion rates of CSs and the LAS were roughly the same in the raw and refined GO. Within standard deviation of data, integrity loss of the 1.4541 SS was the same in both fluids with an order of magnitude lower reaction rates than CSs. So, refining of the raw GO should have no remarkable effect on corrosion rates of steels over medium term at least under the conditions without biomasses. Firm resistivity of the 1.4541 is due to the high chromium and moderate nickel content as the latter decreases sulfidation resistance (Davin A, et al., 1971). Furthermore, from an independent experiment, less favorable activation of metal sulfide formation was recognized and connected to inefficient adsorption and dissociation of the hydrogen sulfide at a pressure of 10 bar without biomasses in the fluid. Then corrosion rates were more affected by the adsorption of dissolved species rather than the gaseous one. Thus, moderate sulfidation resistivity of the 1.4541 in the biomass at low temperature is explained. Roughly the same or somewhat greater corrosion rates with the refining GO along with partial deoxygenation of the acid components must have negligible effect on resistivity of the steels and their corrosion rates up to 250°C.

Table 4. Apparent activation energy, enthalpy, free energy (in kJ mol^{-1}) and entropy (in J mol^{-1} K^{-1}) of sulfide corrosion of steels derived from rate constants (m s^{-1}) based on logarithmic reaction rates (mol m^{-2} s^{-1}) over 24 and 504 hours. Other parameters are the same as detailed in Table 1

Steels	$\Delta E^{\#}_r$ in GO		in GO+WCO		in GO+AWL	
	till 24h	over 504h	till 24h	over 504h	till 24h	over 504h
1.0425	34.4	23.1	33.9	33.0	39.2	36.3
St35.8	32.8	54.8	40.2	40.2	40.7	36.7
1.7335	16.9	30.8	17.9	28.7	28.6	31.1
1.4541	52.5	51.2	53.9	44.2	57.8	54.3
	$\Delta H^{\#}_r$ in GO		in GO+WCO		in GO+AWL	
	till 24h	over 504h	till 24h	over 504h	till 24h	over 504h
1.0425	29.8	18.8	30.0	29.1	34.8	32.0
St35.8	28.3	50.7	35.8	36.2	35.5	32.7
1.7335	12.4	26.1	13.9	24.5	24.0	26.3
1.4541	47.4	46.2	49.5	39.3	53.4	49.9
	$\Delta S^{\#}_r$ in GO		in GO+WCO		in GO+AWL	
1.0425	–326	–355	–324	–338	–314	–331
St35.8	–329	–297	–314	–325	–313	–332
1.7335	–357	–337	–354	–342	–335	–319
1.4541	–307	–323	–309	–339	–291	–314
	$\Delta G^{\#}_r$ in GO		in GO+WCO		in GO+AWL	
1.0425	205	204	203	206	203	205
St35.8	204	206	204	206	204	206
1.7335	204	203	203	203	203	194
1.4541	212	216	215	217	209	214

The Eyring–Polanyi equation (*Evans MG & Polányi M, 1935; Eyring H, 1935; Eyring H & Polányi M, 1931; Laidler KJ & King MC, 1983,* IUPAC, 1997.) was used to estimate thermodynamic balance of formation of transition state and the results are summarized in Table 4. Activation entropy, enthalpy and the Gibbs free energy were assessed with assumption of a gross simplification that the main corrosion process follows a pseudo-mono-molecular mechanism. Regardless of the fluid phases, unfavorable entropy balance in the formation of activated complexes in corrosion of CSs with the increasing temperature suggests corrosion must undergo via a highly associative way as initial steps in reaction of metals with the hydrogen sulfide expected to take place. So, the main reaction route does not favor temperature increase so as adsorption of the reagent and the formation of molecular complexes on the surface. Comparable degree of association on the steel surface should also be unfavorable with elevating temperature as any appreciable compensation in the routes of transition state formation featuring rate limitation was not recognized to occur in GO mixture of the biomasses. The 1.7335 manifested similar behavior in WCO mixture but indicated small decreases of activation entropy in GO and AWL mixture at higher temperature. The former in a medium long-reaction is explained by the fact that this steel develops coherent stable scales of moderate thicknesses in GO (high scaling tendency) and the formation of thick layer of metal sulfides, association of the sulfides at the interface is entropy favored.

A similar but more pronounced balance in the AWL is attributed to the active role of the acidic components in initiation of corrosion via dissociation which is more preferred at higher temperature, and supporting development of thicker scales than in neat GO. Only the 1.4541 indicated progressively decreasing activation entropy barrier from GO through WCO and the AWL mixtures with upper temperatures in comparison with the lower range. This unveils lower proportion of association like adsorption of H_2S and, or greater degree of compensation by dissociation the acidic biomass components promoting corrosion processes above 250ºC. Considering differences of long-term corrosion rates of the 1.4541 over the entire temperature range and the moderately, or insignificantly varied free energy balances, the reaction routes associating with such entropy balances with the increasing temperature are recognized as utmost factor in corrosion kinetics of the high alloy steel in the biomass fuel sources. Alternatively, it should mean corrosion of the 1.4541 SS should not feature significant kinetic control from the gas phase rather composition of the biomass mixed fluids and quality of the scales, bearing in mind that corrosion rates were the lowest in WCO mixture over medium term. In case of the AWL mixture, enhanced corrosion rate with temperature is explained by both the less unfavorable entropy balance of transition states and deteriorated physical, chemical protection function of the scales beyond alteration of the thermodynamic balance of the overall processes.

The Gibbs free energy barriers with the elevating temperature also manifested less favored sulfidic corrosion of steels immersed in the biomasses. Altogether the much lower degree of activation entropy variation with the LAS and the SS compared to CSs as a function of temperature supports the notion that corrosion process should be far less governed by the H_2S. The similarly decreasing activation enthalpy in sulfide corrosion of the CSs points out the lack of valuable barrier function of the scales in ways of less hindered mass transport and activation of interfacial reactions. Decreasing resistance of carbon and LASs to sulfide corrosion at higher temperature is partly connected to catalysis role of the precipitated corrosion products, which also suggests minor variations of sulfide corrosion rates of CSs by the acidic biomass species. Nonetheless, regarding thermodynamic balance of the overall reactions, differences in activation energies of the steels were conversely comparable to the expected free energy changes of metal sulfide formation with iron, nickel and chromium (Barin II, 2008) according to their relative proportions in the alloys.

3.1.2 Time Dependence

As short time results are to define instantaneous thermal activation of sulfide corrosion, data obtained in long term experiments are attributed to kinetic controls. Therefore, logarithmic corrosion rates of the first 24 hours are given in Figures 2.A-D, whereas apparent activation energy besides derived enthalpy, entropy and free energy assessed over temperature between 225 and 300^{o}C are given in Table 4.

Moderate magnitude of initial activation of the 1.0425 and the St35.8 was little affected by the biomasses and time exposure as their activation showed some decrease and increase in GO, respectively. Both with the 1.0425 and St35.8, no changes were found in energy barriers over time by the biomasses, which means the reaction mechanism could only be sensibly altered in GO over time. So, biomasses should have taken part in modifying properties and function of the scales, maintaining 'similar environment' at the steel/fluid interface with time exposure. The lowest initial activation barrier was ascertained to the 1.7335 in GO and WCO blend, which became practically the same in later stage of the experiment and comparable to the ones obtained with CSs. The 1.7335 showed quite similar activation barrier invariable over time in AWL mixture. This partly underscores the fact that neat surface of the LAS is primarily sulfide corrosion sensitive at partial pressure of the H_2S, whereas protection by the scales (indifferent by the fluid phases) seemed only to compensate greater reaction affinity due to the low degree of alloying. The highest initial activation was ascertained to the 1.4541 in WCO and AWL mixtures greater than in GO. Activation energy balance of the transition state showed apparent independence of time exposure in GO and decreasing barriers in WCO and AWL mixtures. Half of the activation barrier at higher temperature pointed out altered thermodynamic balance of SS corrosion in AWL mixture (Table 1) driven by acidic species, decreasing proportion of kinetic control evidenced in the biomasses by time is related to weaker barrier function of the sulfide scale (no such result observed in GO) coupled with some catalytic effect of the biomasses. Invariant activation energy barrier of the 1.4541 over time in GO is attributed to protection by the scales compensating catalytic activity of metal sulfides for further reaction. Decreasing activation energy by time exposure means increasing susceptibility to interfacial processes, less hindered diffusion through sulfide layers is partly construed by assessment performed in the upper temperature range. In case of the St35.8 and the 1.7335, the same tendency of increasing activation in GO should mean certain degree of protection by the scales, whereas the greater initial activation in AWL with decreasing resistance over time unveils catalyzed metal sulfide formation, or less efficient protection by the scales. Enthalpy barrier related heat effect of the activation indicated similar trends and magnitudes of changes. Activation entropy in corrosion of the 1.0425 and the 1.4541 became somewhat greater by time in all fluids, reflecting negative configurational thermal effect of the scales. The lower activation entropy barrier of the 1.4541 also reveals association degree of the reactants in the transition complex increasing over time, which compensated by dissociation related entropy gain in the AWL. The acid, alcohol and water must have minor effect on the formation of metal sulfides. In opposition, the 1.7335 showed a bit decreasing entropy barrier of the activated complex formation (the most in AWL) during scale development. Activation Gibbs free energies mainly reflected entropy balances and so mentionable decrease over time could only be found in corrosion of the 1.7335 in AWL mixture.

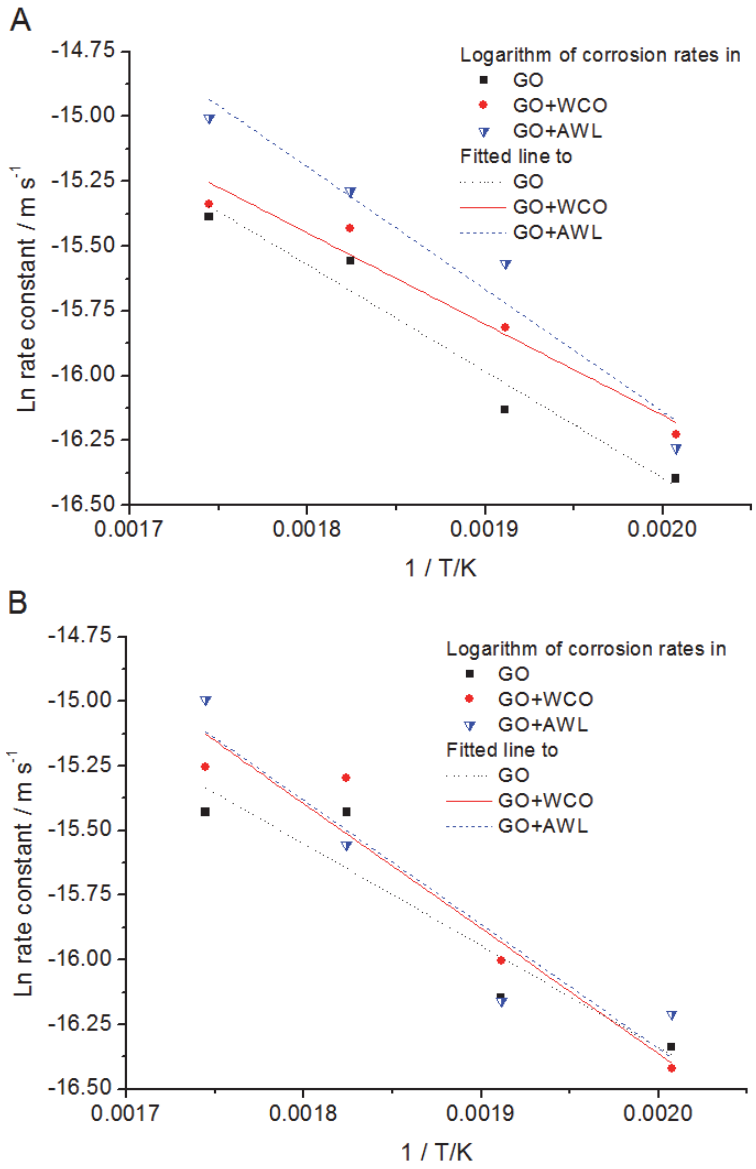
A
Logarithm of corrosion rates in
GO
GO+WCO
GO+AWL
Fitted line to
GO
GO+WCO
GO+AWL
Ln rate constant / m s-1
-14.75
-15.00
-15.25
-15.50
-15.75
-16.00
-16.25
-16.50
0.0017
0.0018
0.0019
0.0020
1 / T/K
B
Logarithm of corrosion rates in
GO
GO+WCO
GO+AWL
Fitted line to
GO
GO+WCO
GO+AWL
Ln rate constant / m s-1
-14.75
-15.00
-15.25
-15.50
-15.75
-16.00
-16.25
-16.50
0.0017
0.0018
0.0019
0.0020
1 / T/K

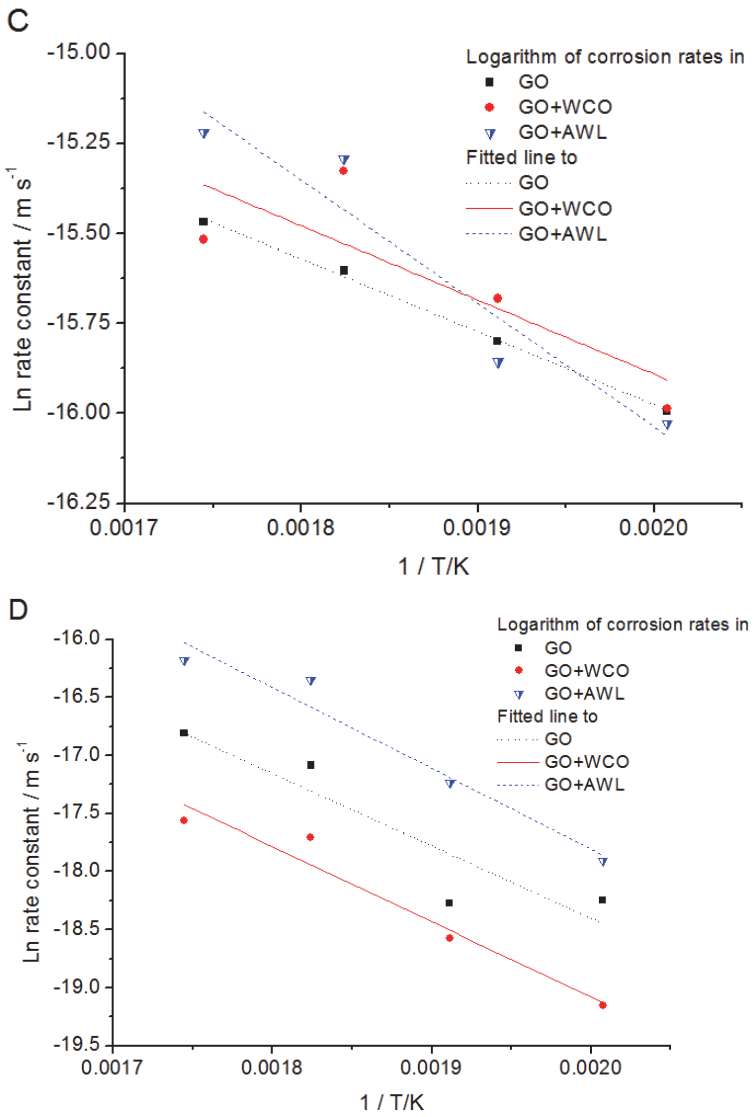

Figure 2. Logarithm of rate constants derived from corrosion rates (expressed in mol m^{-2} s^{-1}) over 24 hours in raw gas oil (GO) and its mixture either with waste cooking oil (WCO) or animal waste lard (AWL) tested at a pressure of 90 bar in the presence of 2 volume% hydrogen sulfide, fittings are over temperature range between 225 and 300°C: A 1.0425, B St35.8, C 1.7335, D 1.4541

In atmospheric corrosion, double logarithm of corroded mass vs. time is for empirical evaluation of reaction kinetics, assessing quality of the corrosion layers. The reaction rates affected by solid-state diffusion through the scales over time should indicate slopes equal or near 0.5, evidencing the presence of pseudo-passive protecting layers. The slopes of around either 0 and 1 mean enhanced barrier nature of the film and losing protection by increased porosity or breakdown of the layer, respectively. In this work, double logarithm of corrosion rates and time is used for data evaluation over the 504h period. Thus, data are presented in Figures 3.A-D and integral slopes in Table 5. The more negative values reflect evolution of firm barrier behavior, whereas the less negative ones mean rather inefficient barrier protection. As useful information, the type of failure leading to inefficient protection can be recognized by differential reaction rates (base on mass losses) expressed as hypothetical scale thicknesses between time periods are given in Figures B2.A-D. The latter indicates breakdown of scales via loss of coherence in the form of cracking or spalling failure. Integral slopes obtained for the 1.0425 revealed low protection in GO and a somewhat better rate deceleration in WCO and AWL mixtures. In addition, the least valuable barrier function evolved at 250°C in all fluids which is partly in line with lower thicknesses of the coherent scales. The slopes over partial time intervals (Figure 4.A) indicate more pronounced deceleration of reaction rates from late to early stages of the experiments at elevated temperature.

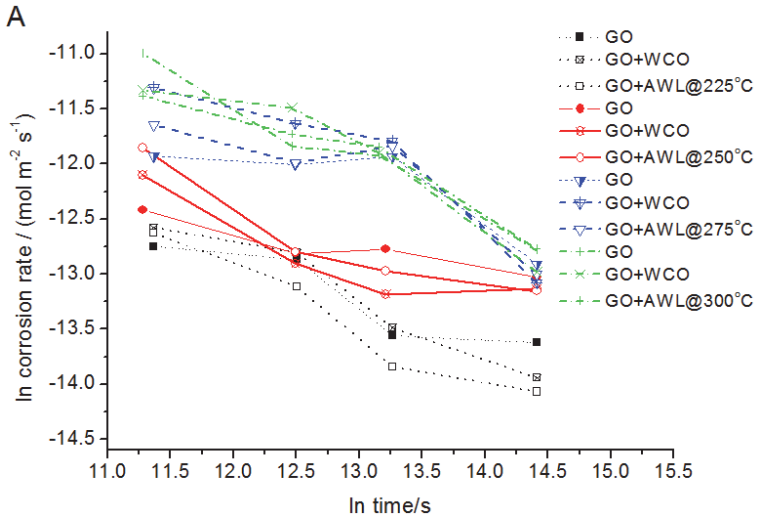
A
ln corrosion rate / (mol m-2 s-1)
ln time/s
GO
GO+WCO
GO+AWL@225°C
GO
GO+WCO
GO+AWL@250°C
GO
GO+WCO
GO+AWL@275°C
GO
GO+WCO
GO+AWL@300°C

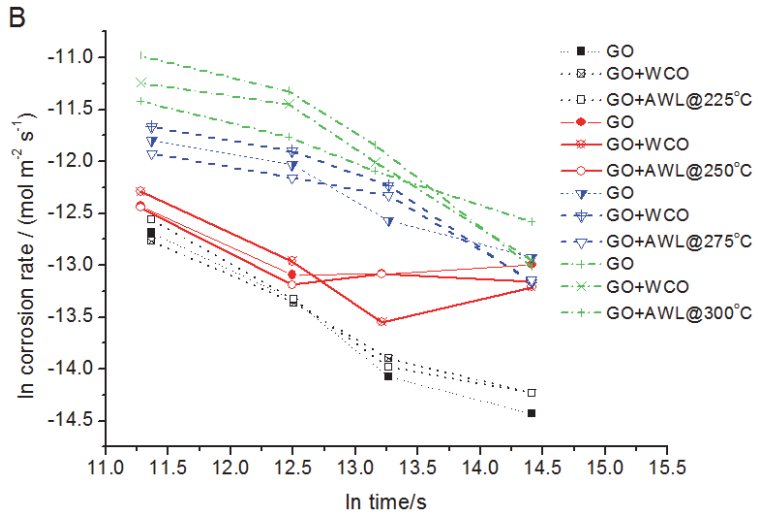
B
ln corrosion rate / (mol m-2 s-1)
ln time/s
GO
GO+WCO
GO+AWL@225°C
GO
GO+WCO
GO+AWL@250°C
GO
GO+WCO
GO+AWL@275°C
GO
GO+WCO
GO+AWL@300°C

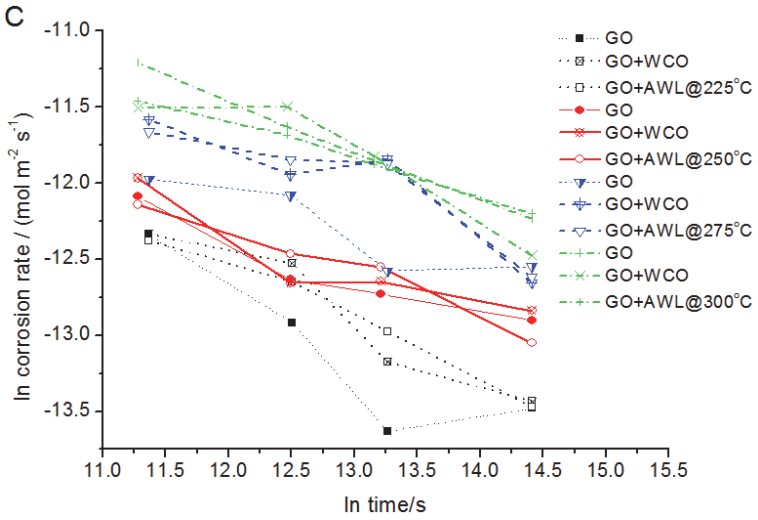
C
ln corrosion rate / (mol m-2 s-1)
ln time/s
GO
GO+WCO
GO+AWL@225°C
GO
GO+WCO
GO+AWL@250°C
GO
GO+WCO
GO+AWL@275°C
GO
GO+WCO
GO+AWL@300°C

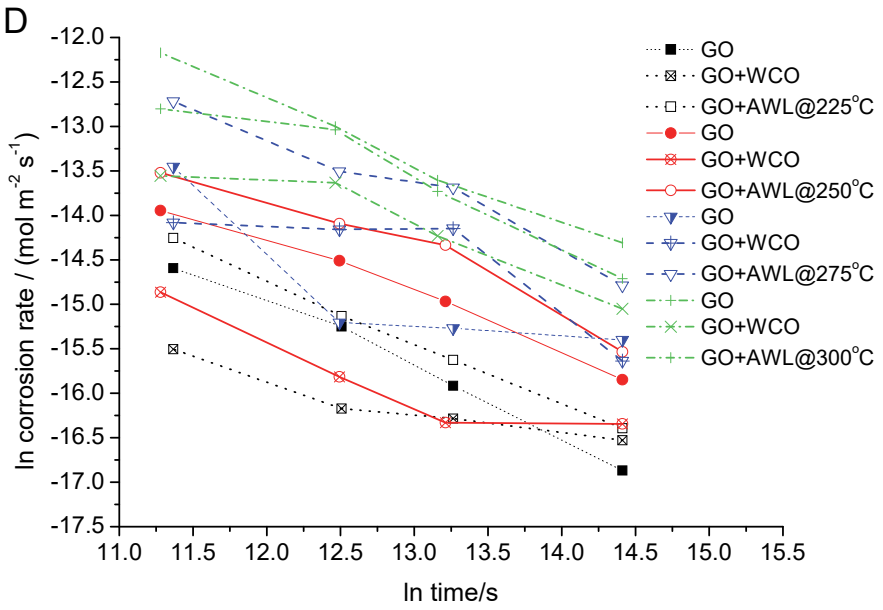

Figure 3. Double logarithm of integral corrosion rates in raw gas oil (GO) and its mixture either with waste cooking oil (WCO) or animal waste lard (AWL) tested at a pressure of 90 bar in the presence of 2 volume% hydrogen sulfide: A 1.0425, B St35.8, C 1.7335, D 1.4541

The 1.4025 should have developed scales with thicknesses of 25 23 and 29 μm as integrated corrosion rates over 168 hours at 275°C but measured layer thicknesses were 10.5, 39 and 31 μm in GO and the WCO and AWL mixtures (Table 2), respectively. This means spalling failure of the scales must have occurred more frequently in GO (owing to higher brittleness) than in WCO and AWL mixtures in which thicker scales formed without layer detachment over a week along with some soot deposition. Besides the temperature, scaling tendency of the 1.0425 was assisted by the biomass components in a way of longer time constant of spalling failure. This should mean the formation of more porous, less compact and less brittle, more ductile scales in biomasses at roughly the same corrosion rates of the steels in GO. The time constant to cracking and spalling failure decreased with the increasing temperature as corrosion rates recovered within shorter times. The relationship between time of crack or spall and temperature is probably the same as exponential increase of the corrosion rates but this could not be defined exactly due to low sampling rate of the corrosion rates over time. The St35.8 experienced similar degree of deceleration of corrosion rates over time, except for the ones measured at 250°C (Figure 4.B). At 225°C, better protecting scales formed continuously in the first 168 hours then corrosion rates rapidly converged to constant levels with the lowest slopes at 250°C in all fluids, which means integrity loss is not dominantly ruled by mass transport through the scales. Hypothetical differential corrosion rates normalized over hour periods manifest occasions of spalling up to 250°C, continuous formation and moderate protection at 275 and pseudo-passivating effects at 300°C within less than 168 hours. So, the temperature assisted faster formation of better protecting scales on the St35.8 than the 1.425 at similar rates of integrity loss suggests higher corrosion resistance of the St35.8. The 5, 12 and 13 μm theoretical scale thicknesses with the St35.8 over 168 hours at 275°C was far inferior to the ones (16, 31, 33 μm) measured with soot deposition.

Barrier protection of the St35.8 is due to the more compact microstructure and lower porosity of the scales. The 1.7335 indicated low variation of integral slopes as a function of temperature and composition of the fluid phases, not reaching pure rate limitation by diffusion control in solid state in either case. The high scaling tendency, high corrosion rates and the less steep integral slopes along with their continuously decreasing manner over time periods (approximately the same decreases, Figure 3.C) give the sense of negligible degree of passivation by the scales regardless of temperature and liquid phase. Deficient scaling tendency of the 1.7335 is also pointed out by comparison of theoretical (6, 28, 25 μm) and practical (13, 35, 27 μm) thicknesses of the scales obtained after 168 hours at 275°C. Hence, spalling failure resulted in half layer thicknesses in GO, whereas soot deposition and pure metal sulfide layers with more ductility formed in WCO and AWL mixtures, respectively. These also mean less effective barrier function of the scales on the 1.7335 LAS. Non-continuous layer formation and some spalling

failure took place at all temperature in all fluids. The 1.4541 indicated continuously decreasing reaction rates over time (Figure 3.D) in connection with good protection at almost all temperatures (Table 5). Reminding observation results of structural differentiation of the scales on SS with at least two layers of an inner adherent and an outer incoherent one, protection behavior must feature physical and chemical sorts and hypothetical scale thicknesses denote recover of corrosion rates by time regardless of the fluid phases, which support the idea of partial failure of the pseudo-passivating layers. The highest degree of layer failure, variation of the corrosion rates was experienced in GO at 300°C. This is explained by low corrosion rate of the SS and low stability of scales, resulting in less advanced scaling tendency. As for the integral slopes, pseudo-passivating role of the scales was assisted by the elevating temperature and showed increasing tendency of layer formation by the presence of biomasses, even though thicker scales rarely lead to progressive protection probably because of their higher porosity.

Table 5. The slopes of logarithmic corrosion rates over 504 hours as a function of logarithm of time (expressed in seconds). Other parameters are the same as detailed in Table 1

Steel alloys	raw GO	GO+WCO	GO+AWL
1.0425			
225°C	–0.32	–0.47	–0.50
250°C	–0.18	–0.33	–0.41
275°C	–0.30	–0.56	–0.40
300°C	–0.43	–0.53	–0.53
St35.8			
225°C	–0.60	–0.49	–0.57
250°C	–0.17	–0.32	–0.21
275°C	–0.39	–0.49	–0.39
300°C	–0.38	–0.56	–0.66
1.7335			
225°C	–0.41	–0.39	–0.36
250°C	–0.25	–0.26	–0.28
275°C	–0.22	–0.32	–0.30
300°C	–0.24	–0.32	–0.33
1.4541			
225°C	–0.70	–0.32	–0.70
250°C	–0.42	–0.49	–0.63
275°C	–0.60	–0.48	–0.65
300°C	–0.63	–0.50	–0.69

The loss of barrier function as a sign of sensitivity to composition of the fluid phases was recognized in later stages of experiments at a relatively high partial pressure of the H_2S. Hydrogenising refining of the small biomass molecules is unlikely to occur under applied conditions without good catalyst (Kubicka D & Horacek J, 2010; Walendziewski J, et al. 2009). So, deteriorated barrier function and the less effective scale formation at high corrosion rates of the CSs and LAS are not primarily connected to fluid phases, only in case of the 1.4541 SS. Spalling failure of incoherent brittle scales was reflected by the large amount of debris gathered from bottom of the sample holder glasses even at the end of 24 hours experiments above 250°C. Difference between corrosion resistance of steels and protective nature of the scales is underlined by the fact that one tenths of layer thickness results in greater deceleration of corrosion rates with the 1.4541 than ten times thicker scales on CSs and a LAS. Increasing temperature lead to decreasing variation of the higher reaction rates as function of time and type of the biomasses. The presence of biomass generally entailed in reduced changes of the reaction rates over time. So, protective nature of the sulfide scales should not be comparable to the ones formed in GO. Hence, unlike raw GO biomasses seemed to assist maintaining higher corrosion rates primarily by degrading barrier behavior of the scales. Time dependence of differential and integral corrosion rates unveiled development of either coherent films with varied porosity or continuous formation of compact scales affording good physical and chemical protection by time but undergoing through spalling failure on periods depending on plasticity, brittleness of the films.

3.2 X-ray Diffraction

Diffraction pattern of troilite, 1:1 stoichiometric ratio of iron sulfide (FeS) was identified as a majority in spalled scale of the 1.0425 tested in GO (Figure C1.A). The scale was composed of sulfide deficient corrosion product

and low crystalline metallic iron featuring high magnetic susceptibility in ~1 wt.%. The low intensity reflections at 17.5° and 30°/2θ are obviously not related to mackinawite because this phase transform to more stable pyrrhotite, troilite sub-phase over time. Troilite is more stable in acidic solutions under reducing environment (below the $H+/H_2$ equilibrium line, Schoonen MAA & Barnes HL, 1991). In addition, greigite is no way to attribute to the reflections at 30 and 53°/2θ. Although pyrrhotite was present in scales, showing overlapping features with the metallic phase (Csákberényi-Malasics D, et al., 2012), the intense reflection at 44°/2θ is assigned to poly-crystalline iron (Saw CK, et al., 2006). Different diffraction pattern of metal sulfide (b) is noticed by varied intensity ratio of reflections at 43° and 53°/2θ. This owes to composition change of scales having metallic iron besides crystalline troilite (FeS). So, some metallic iron remained in corrosion products without full conversion to metal sulfide in refined GO over 504 hours. Long-term exposure favored high sulfide conversion of iron and growth of crystals in raw GO having high sulfur content. The same reaction rates resulted in the evolution of similar amount of scales in refined GO, which proved to be more brittle. Higher proportion of scales spalled besides rapid disintegration of metallic iron. XRD investigation of scales formed on the 1.7335 showed diffraction pattern (c) similar to the 1.0425 (b) tested under the same condition. Nevertheless, greater amount of porous scale detached less frequently, allowing seldom surface renewal for further attack and some diffusion hindrance to accessing the metallic surface by sulfide species. As an overall, there was a minor contribution by the fluid phases with species of sulfur content on sulfide corrosion of the CSs.

Diffraction pattern of scales on coupons of the St35.8 tested in GO (Figure C1.) exhibited lower degree of crystallinity of iron sulfide appeared to be dull blackish first outer layer. The reflection at 44.8 with a minor feature at 65.2°/2θ give the impression of metallic residues in the corroded layer, or might be some gain from the metallic phase underneath the scale with thickness of ~16 μm. Different diffraction pattern of the St35.8 tested in AWL mixture of GO was obtained from outer scale layers of light grey color, indicating no signs of metallic iron (b) at a thickness of 33 μm. The intense reflections at 17, 18.6, 29.7, 33.5, 35.3, 41.8, 43.0, 46.9, 53.0 and 65.3°/2θ with type of the pattern means highly crystalline troilite in majority. More crystallized metal sulfides developed in acidic waste lard (the same experienced in WCO) than in raw GO leaving thick layers of coke and graphitic layers (see Raman analysis results) on top of the sulfide covered coupons.

3.3 SEM and EDX Analysis

Morphology of the corroded surface with coherent scales at the solid-fluid interface is presented in Figures 4.A-C, whereas measurement and data evaluation results are in Table 6. The 1.0425 exhibited moderately uneven surface (Figure 4.A) with signs of porosity scattered in low density on the surface. In WCO mixture, sulfide layer in a thickness of ~1.25 μm developed in stable manner by time on the randomly oriented polycrystalline surface. A film with greater thickness was mechanically unstable at integral corrosion rate of 0.06 mm $year^{-1}$ so outer layers detached. Scales on the St35.8 showed fine crystal structure without observable porosity, micron-size pores (Figure 4.B) which is partly due to the finer grain structure of the St35.8 steel matrix than the 1.4025 features. No signs of local attack were observed on surface of the St35.8 in opposition with the 1.0425 exhibiting severe pitting type local damages at a general corrosion rate of ~0.05 mm $year^{-1}$.

Table 6. Elemental composition (in atomic%) and thickness of coherent scales (calculated with the density of 4.80 g cm^{-3}) developed in mixture of gas oil and waste cooking oil tested at a pressure of 68 bar for 98.5 hours, composition of corrosion products removed from surface of the 1.0425 carbon steel coupons immersed raw gas oil at a pressure of 90 bar for 504 hours, all at a temperature of 250°C

Elements	1.0425	St35.8	1.7335	1.4541	1.0425
Thickness (μm)	1.25	0.50	1.43	0.06	
The ratio of coherent and spalled scales	1.4	0.6	2.1	6.0	
The ratio of coherent and hypothetical scale thicknesses	0.57	0.36	0.68	1.00	
O (K)	-	-	-	-	6.02
Si (K)	0.97	-	0.97	-	0.00
S (K)	0.68	0.87	6.94	-	36.58
Cr (K)	-	-	1.49	-	-
Mn (K)	0.54	1.40	0.88	-	1.06
Fe (K)	97.81	97.73	89.72	-	56.33

Besides the metallurgical aspects of microstructure relating to changing fineness of the grain size, double

manganese amount of the 1.0425 compared to the St35.8 (forming high concentration of sulfide inclusions in the metal lattice) is connected to low pitting resistance of the former. Uneven island-like distribution of the good cathodic pearlite phase (due to effective depolarization to hydrogen ion discharge) at micron-scale led obviously to higher sulfide conversion rate of the ferritic phase around edge of the porous layers by galvanic coupling (Kim SJ, et al., 2016). Incompact, incoherent scale formation is reflected in high variation of the low layer thickness, maintained at the same corrosion rate as the St35.8. The 1.7335 showed continuous layer formation with large epitaxy domain size of the corrosion products having pores of small size (Figure 4.C). The susceptibility to form stable scales in time is noted by mass of the layers (sampling at a time of the experiment) with a geometrical layer thickness of ~1.43 μm formed at a rate of 0.06 mm year^{-1} which was one of the highest of all cases.

The scale having theoretical layer thickness of ~60 nm could form on the 1.4541 at a rate of less than 2 μm year^{-1} thanks to its high resistivity more than an order of magnitude lower than most of the layer thicknesses on CSs and LAS. The results unveiled the SS was only one yielding 0.91 (close to unity) as a ratio of layer thicknesses of the real and hypothetical ones (based on complete mass loss of the metallic phase) which means most of the corrosion products remained on the surface during the experiment opposed to that of CSs exhibiting ratios between 0.36 and 0.68. Other high alloy steels gave values above unity with the meaning of only weight gain by sulfide corrosion. The ratio of one is more approached the less susceptibility of the scales is to spall in a way of relaxation of the mechanical stresses. With exception of the 1.4541 SS not providing enough quantity of corrosion products in layer thickness for EDX analysis, investigation of the CSs and LAS provided the following results. Less than 1 atomic% of sulfur could be measured on surface of the 1.0425 and the St35.8, partly due to low thickness of the scales, whereas 7 atomic% of sulfur was detected on the 1.7335 thanks to the uniform layer structure. Nearly the same layer thickness on the 1.0425 and the 1.7335 (1.25 and 1.43 μm) means metallic iron content is considerably higher in scales on the 1.0425 than that on the 1.7335, in accordance with the XRD results. In other words, sulfide conversion of the disintegrated metallic iron was higher with the 1.7335 than the 1.0425 in the scale development process. It also means chemical and mechanical erosion corrosion of the steels took place at a rate of 0.05 mm year^{-1} and above during collapse of the metallic lattice then further sulfide conversion of metallic iron must have been undergoing. Even after three weeks in GO at 250ºC and 90 bar, 20 atomic% iron was detected in the scales by EDX (highly magnetic as amorphous iron) than stoichiometric quantity of sulfur besides the chemically corroded iron sulfide of 36.6% (assumed being in 1:1 ratio as FeS) in coherent layers removed from surface of the 1.0425 coupons.

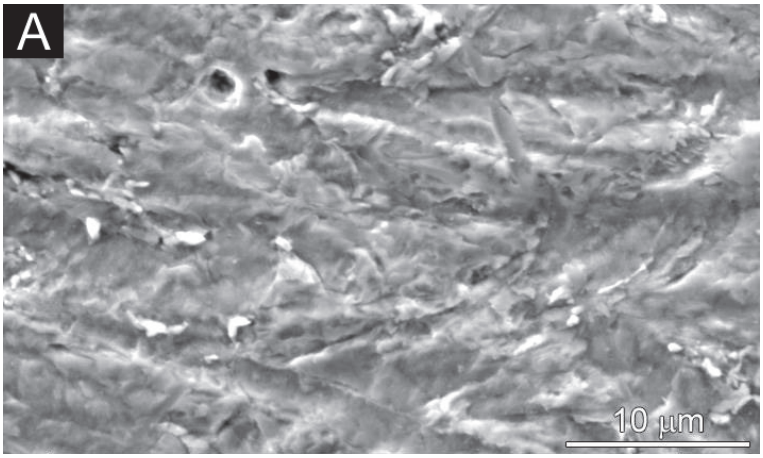

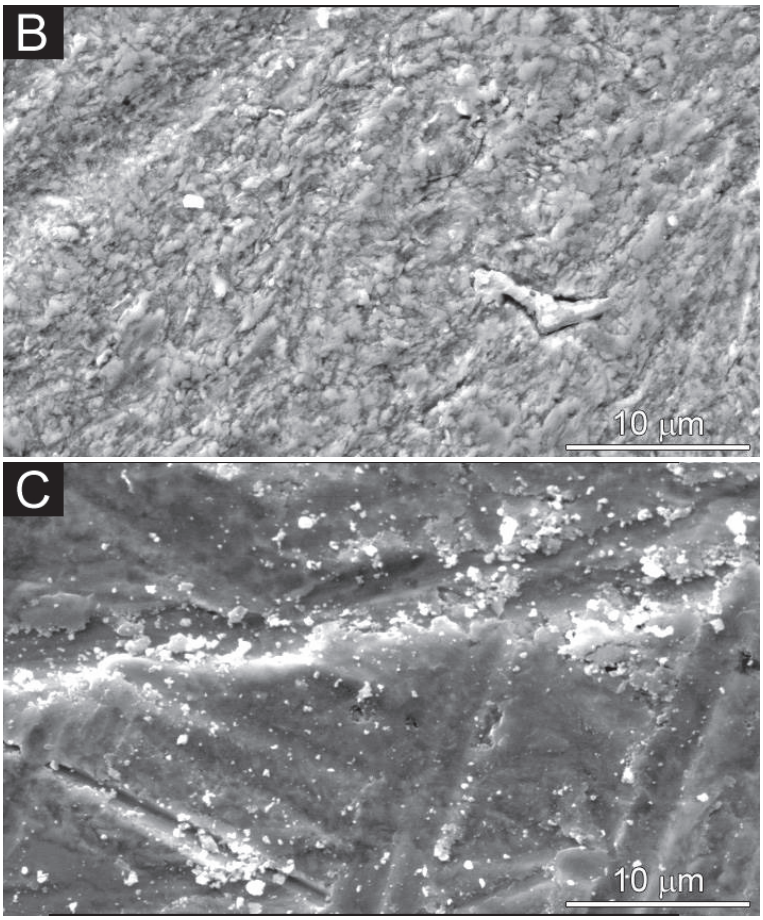

Figure 4. SEM micrographs of the carbon and low alloy steels tested in waste cooking oil mixture of gas oil at 250°C for 98.5 hours under the pressure of 68 bar: A 1.0425, B St35.8, C 1.7335

This can only be explained by higher corrosion rate of CSs along grain boundaries inward the metal lattice (with incomplete sulfide conversion of the metal) than general corrosion of the 1.4541 high alloy steel via homogeneous sulfide conversion of the surface atoms. This assumption is thought to be confirmed by enhanced barrier nature of the scales on the 1.4541 than much thicker but far less protective films on the LAS. The free energy change of sulfide corrosion in absolute value is inferior to diffusion activation in solid state at low temperature of ~200°C. Therefore, high general and local corrosion rates of CS and LASs could only occur by short-cut diffusion along grain boundaries and dislocations than lattice diffusion and phase boundaries. Molar ratio of the iron sulfide and metallic iron was between 3:1 and 1.8:1 in the brittle and porous scales. Detached and crumbled iron sulfides showed domain dimensions of lateral size of ~500 μm and thickness of ~10 μm. Sulfide layers should primarily grow with outward transport of cations to the scale/gas interface which leads to accumulation of low internal stresses. As one of the four stress-relief mechanisms, spalling breakdown of the scales means coherence failure experienced with thicker scales on CSs at 300°C in the first 24 hours. Maximum-stress affects metal/scale interface with thin scales. On non-flat surfaces, geometry of the coupons might also be the source of scale detachment (Hancock P & Hurst RC, 1974). Films over levelled interfaces are less susceptible to spalling compared to the ones with low radii, high curvature at inner and outer edges of the coupons (Evans AG & Hutchinson JW, 1984). Low ductility at low temperature and high corrosion rates should inevitably lead to spalling and detachment, breakdown of the scales.

3.4 Optical Microscopy

Micrographs taken from surface of both sides of the 1.0425 coupons after scale removal are presented in Figures 5. Near edge of the coupon of one side (Figure 5.A), densely populated pits were observed on the surface independent of type of the fluid phase. This side of the coupon was placed upwards in the glass type sample holders, directly sensing and responding to the attack of the H_2S. At such a high local damage concentration, there is no validity to discern corrosion around inclusions (in initial phase of the experiment at the same concentration on flip-

side too) and grain boundaries. On flipside of the coupons (Figure 5.B), pits with much lower density were on the surface. No other steels experienced such a local attack and this result also confirms corrosion of the CS and LASs are governed by the H_2S at high partial pressures. The sulfide corrosion caused high density pitting was without preference of phases or boundaries in the metal lattice and inclusions, aside from a somewhat higher damage density around outer rim of the coupons. Other side of the coupons showed the same kind of damages with similar depth of the attack but at a considerably lower surface density. Beyond inhomogeneous nucleation of pits on surface of the 1.0425, the St35.8 never showed such a local damage. Considering compositional difference between the 1.0425 and St35.8 CSs with around doubled manganese content of the former, the phenomena of sulfide pitting is connected to the formation and further reaction of the manganese sulfide inclusions in the 1.0425, corresponding to the literature (Kim SJ, 2016). Sulfide pitting on backsides of the coupons led to regioselective sulfide derivatization of the steel as local concentration of the H_2S was slightly lower compared to the one sensed by the frontal sides, leading to differentiation of reaction routes based on the regions of critical alloying elements and crystal boundaries.

Temperature plays vital role in accelerating acidic corrosion both chemically and electrochemically (Slavcheva E, 1999) but activation of the former is more thermal dependent so as dissociation of weak acids and dissolution of the corrosion products are more preferred at elevated temperature (Wu XQ, 2004). Owing to the limited range of galvanic coupling because of the very low electrical conductivity of the fluids, the electrochemically accelerated corrosion must result in local actions such as pitting (like sulfide driven corrosion of the 1.4025 regardless of the fluid phase), whilst acidic corrosion at lower temperature leads to general processes like uniform etching and polishing of metals. The latter was experienced with all steels in WCO mixture in the absence of hydrogen sulfide.

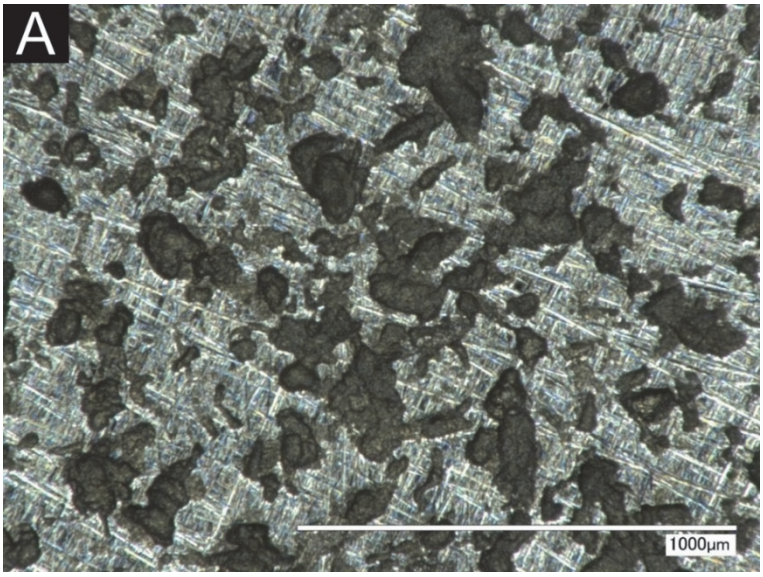

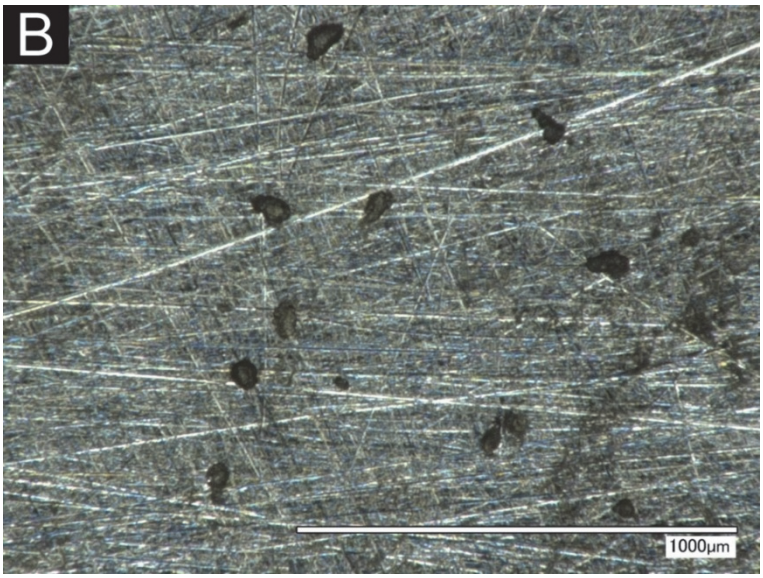

Figure 5. Microscope images of the 1.0425 carbon steel of the A front and B flip side of the coupons immersed in waste cooking oil mixture of gas oil tested at 250ºC for 168 hours

3.5 Micro-Raman Spectroscopy

Raman spectra of scales removed from surface of the coupons tested for times of 8, 20 and 24 h and 98.5 h at 250ºC are presented in Figs. 6.A and B. In short time experiments (Fig. 6.A), low Raman intensity near threshold of the signal to noise ratio are due to low quantity of the corrosion products. The 1.0425 (A) showed a rather featureless spectrum. The upper region was nearly identical to that of the St35.8 (B) and the 1.7335 (C). In the low wavenumber region of 150-800 cm^{-1}, spectrum of the 1.0425 was similar to the one detected to the 1.4541 (D) with the only exception of a strong feature in the wavenumber region of 550-800 cm^{-1}. Because bleak feature of the spectra around the characteristic wavenumbers, crystalline troilite (Wang H & Salveson I, 2005) must have been in small proportion on the St35.8 and the 1.7335 (lines at 289 and 290 cm^{-1}). Metal sulfides, detected in a somewhat greater proportion of crystallinity (in a small scale amount) on the slower corroding 1.4541, is attributed to the more pronounced feature in the wavenumbers of 550-800 cm^{-1}. The intense broad and weak features at 1292 and 218 cm^{-1} were probably troilite on the St35.8, 1.7335 and the 1.4541, which is in accordance with the literature data (Ma C, et al., 2012). Low crystallinity of sulfides is due to the short time of development. The Raman features of troilite, a weak one at 456 cm^{-1} and sharp ones at 600, 398, 283, 600, 400 and 295 cm^{-1} were not found (Xie X & Chen M, 2016). The wavenumbers of moderate intensity at 321, 317 and 315 cm^{-1} means mackinawite (Lennie AR, et al., 1995) on the 1.0425, St35.8 and 1.4541, which evolves in initial phase of corrosion, appearing as intense overlapping peaks between 310 and 320 cm^{-1} depending on degree of crystallinity (Rémazeilles C, et al., 2010). Thus, greater reaction rates lead to low crystalline product as the rate of nucleation surpasses orientation and growth. Insignificant intensities between 280 and 300 cm^{-1} (206 257, 296 cm^{-1} and the 256, 312, 355 cm^{-1}) and in the region of 350-360 cm^{-1} are connected to mackinawite ($Fe(II)S_{1-x}$ and $Fe(II-III)S_{1-x}$) and iron-rich mackinawite, respectively (Colomban P, 2011). On the 1.4541, the very low intensity at 240 cm^{-1} is attributed to chromium rich troilite, whereas the low intensities at 255 (290) and 365 cm^{-1} is assigned to protective layer composed of daubrelite ($FeCr_2S_4$ and Cr_2S_3). These phases could be in very low proportion because of none of the XRD results confirmed their presence irrespective of thermodynamic stability regions. In the medium-long term tested samples (Figure 6.B), metal sulfides were measured with high intensities but partly because of the gradually underwent processes most of the main Raman features could not be resolved. Detection of troilite by overlapping features of 283 and 295, the strong signal at 456 and cm^{-1} and a weak one at 220 cm^{-1} were unanimous in all samples. The overlapping peaks in the region of 200-400 cm^{-1} tell that scales on the 1.4541 were particularly rich in troilite and mackinawite. The broad feature at 1292 cm^{-1} and the ones at 600 and 398 cm^{-1} ordinarily expected to detect were not found in either spectrum. The intensities at 321, 317 and 315 cm^{-1} are associated with mackinawite on all steels, as an intermediate transforming continuously to more stable troilite.

The Raman spectra of the scales on steel samples tested at 275ºC for 168 hours are presented in Figures 6.C and D. The spectra of high intensity Raman signals with appropriate signal-to-noise ratio is due to abundance of the corrosion products. The intense bands overlapping in the regions of 280–300 and 312–325 cm^{-1} are connected to

the mixture of troilite and mackinawite. At least four high intensity carbon bands were identified between the wavenumbers of 1100 and 1200 cm^{-1} on the 1.4541 and darker side of the St35.8 because of the higher quantity of soot deposition. The three, D1 (at 1350 cm^{-1}), G (at 1580 cm^{-1}) and D2 (at 1620 cm^{-1}) bands of carbon appeared with shoulders between 1700 and 2000 cm^{-1} better separated in spectra of the 1.0425 and the 1.7335. In other aspects of nano- and micro-structure of allotropes in relation with graphitic crystallization of deposited carbon on steel coupons, a single band at 1575 cm^{-1} stems from single crystals of graphite, whereas stress-annealed materials such as pyrolytic graphite, activated charcoal and vitreous carbon are detected at 1355 cm^{-1}.

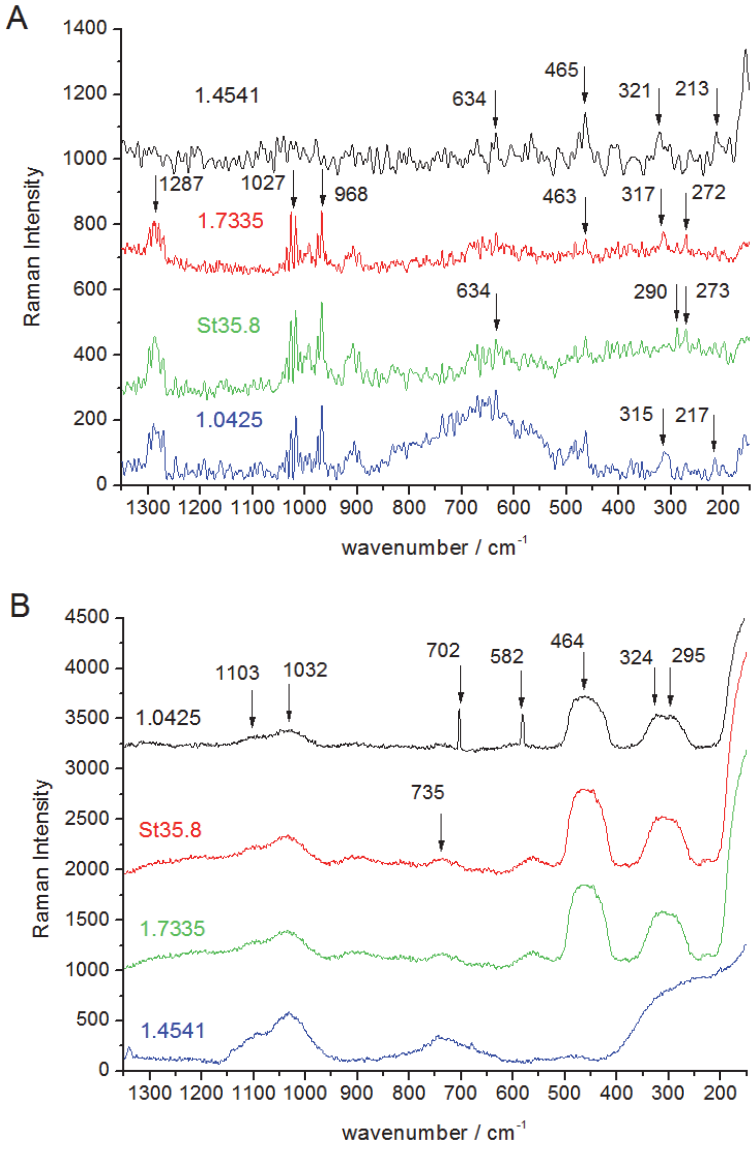

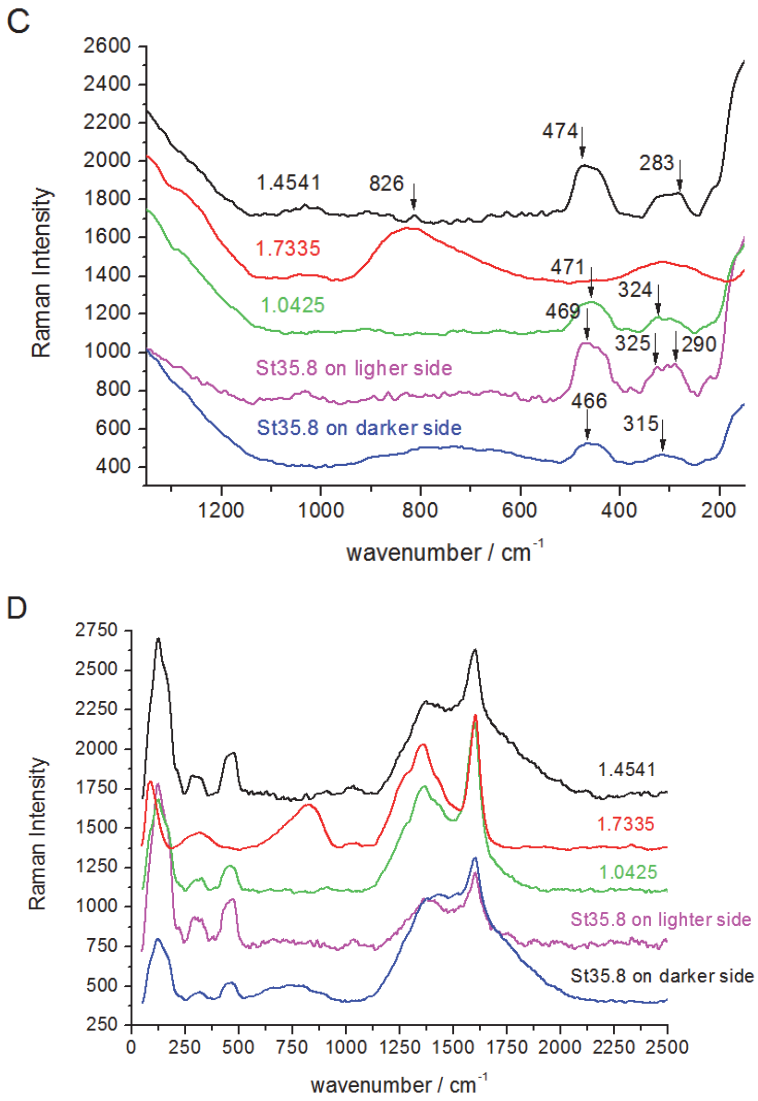

Figure 6. Micro-Raman spectra A of steel alloys tested in gas oil under conditions as stated: 1.0425 (250ºC/20bar, 8h), St35.8 (250ºC/50bar, 24h), 1.7335 (250ºC/20bar, 8h), 1.4541 (250ºC/50bar, 24h), B steel alloys tested in WCO mixture at 250ºC, 68 bar for 98.5 hours, C and D steel samples tested in WCO mixture at 275ºC, 90 bar for 168 hours over different wavenumber ranges

Raman intensity of the latter is inversely proportional to crystallite size and intensity of the band allows estimation of crystallite size in carbon layers. Low crystallinity of the sulfide products and carbon deposition owes to low temperature of the experiment besides the short time exposure. Amorphous iron sulfides formed in the induction periods were less coherent, more susceptible to spall than the more crystallized ones evolved in slower reactions. Induction time to scale is probably very low at a pressure of 25 bar but crystallization requires longer times. Thus, time constants of spalling failure relating to relaxation of accumulated stresses are probably faster than crystallization of the iron sulfides. In case of troilite, it shall be longer than 8 hours but much less than 504 hours at 250ºC and pressure of 90 bar. Phase transformation to troilite occurred within hours at 250ºC. Pyrrhotite formation might need couple of days so its detection after 3 days is expected. In our experiments, not exactly in line with the pyrrhotite-troilite transition boundary (Shoesmith DW, et al. 1980; Wikjord AG, et al., 1980), elevated temperature favored troilite formation rather than pyrrhotite at 2 bar partial pressure of the H_2S. In fact, (Rickard D & Luther GW, 2007), based on kinetic reasons of the high reaction rates without mass transport control (Ren C, et al., 2005), generally mackinawite forms first almost no matter of conditions (Smith SN, 2015) then it transforms later due to thermodynamic reason. If there is any metastable cubic FeS it should also transform to pyrrhotite, troilite over time (Choi HJ, 2006) in the presence and absence of chloride (Dehkordi EH, 2007).

4. Conclusions

The high rate of sulfide corrosion of carbon steels in the temperature range of 200 and 300ºC is insignificantly impacted by the biomass fuel sources. Acidic components of the biomasses did not contribute either by chemically and electrochemically to the overall corrosion processes in a comparable proportion. Modification of the sulfide scales by the biomasses resulted in somewhat better barrier protection of the CSs but it does not lead to enhanced protection over long-term. Low steady thickness of the scales in GO is due to frequent cohesive failure, while higher scale thickness in biomass mixtures is connected to lower brittleness, increased ductility. The low alloying of steel does not improve high sulfide corrosion resistance and inefficient protection of porous scales, even though low alloy steel develops thick and cohesive sulfide layers. Preferred formation of thick non-compact sulfide layers with temperature is reflected by less unfavorable entropy balance of the activated complexes. Catalytic effect of the metal sulfides for further corrosion was found to balance protective nature of the films by time unless the scales are susceptible for frequent breakdown, spalling type cohesion failure. The orders of magnitude lower corrosion rate of stainless steels in neat gas oil is considerably impacted by the acidic biomass components of waste cooking oil and animal waste lard. So, increases of the corrosion rates with temperature were similar to that of carbon steels. This phenomenon is explained by the less unfavorable entropy and Gibbs free energy balance between the initial and transition states of the reactants with the increasing temperature. High sulfide corrosion resistance of the 1.4541 SS considerably lowered by the biomasses, which is reflected in the overall thermodynamic balance by time exposure rather than less hindered kinetics. The high corrosion rates allowed us to conclude low proportion of the biomasses with high free fatty acid contents should be lower than 10 wt.% to avoid fast integrity loss of stainless steels.

Acknowledgements

This work was supported by the GINOP-2.3.2-15-2016-00053 project with title of "Development of engine fuels with high hydrogen content in their molecular structures (contribution to sustainable mobility)". Authors are indebted to Makó Éva for the XRD measurements. Kovács Kristóf is gratefully acknowledged for the optical microscope measurements. Authors are thankful to Tóth Csaba, who worked at the Department of MOL Hydrocarbon and Coal Processing, Institute of Chemical and Process Engineering, the University of Pannonia, for his variety of contributions to the experimental work. Authors are grateful to Balázs Margit (Bay Zoltán Nonprofit Ltd. for Applied Research) for lending the analytical results of the biomass fuel sources.

References

Arrhenius, S. A. (1889). Uber die Reaktionsgeschwindigkeit bei der Inversion von Rohzucker durch Sauren. *Z Phys Chem, 4,* 226-248.

Barin, I. (2008). Thermochemical data of pure substances, VCH Verlag, Weinheim, Germany. https://doi.org/10.1002/9783527619825.ch3

Choi, H. J., Al-Bannai, N. S., Al-Beheiri, F. I., & Warnken, D. K. (2006, March). NACE International Corrosion Conference, Paper no. 653, San Diego, California, US, 1-10.

Colomban P. (2011). Potential and drawbacks of raman (micro)spectrometry for the understanding of iron and steel corrosion, chapter 28th. In: Chiaberge M editor. New trends and developments in automotive system engineering. InTech Europe, Rijeka.

Craig, W. K., & Soveran, D. W. (1991). Production of linear alkanes by hydrotreating mixtures of triglycerides with vacuum gasoil. US Patent 4 992 605.

Csákberényi-Malasics, D., Rodriguez-Blanco, J. D., Kovács, K., Viktória, R., Benning, A. L. G., & Pósfai, M. (2012). *Chemical Geology 294-295,* 249-258. https://doi.org/10.1016/j.chemgeo.2011.12.009

Davin, A., Coutsouradis, D., & Habraken L. (1971). Influence of alloying elements on the hot-corrosion resistance of Co-Cr alloys. *Materials and Corrosion, 22,* 517-527. https://doi.org/10.1002/maco.19710220609

Dehkordi, E. H., & Tavakoli, A. R. (2007). The effect of time on the formation and growth of passive layer on carbon steel A516 GR.70 in sour water. *International Journal of Iron Steel Society Iran 4,* 28-33.

European Committee for Standardization, Standard EN 590:2004, (2004). *Automotive fuels – diesel – requirements and test methods*.

Evans, A. G., & Hutchinson, J. W. (1984). On the mechanics of delamination and spalling in compressed films. *International Journal of Solids and Structures 20,* 455-466. https://doi.org/10.1016/0020-7683(84)90012-X

Evans, M. G., & Polányi M. (1935). Some applications of the transition state method to the calculation of reaction

velocities, especially in solution. *Transactions of the Faraday Society, 31,* 875-894. https://doi.org/10.1039/TF9353100875

Eyring, H. (1935). The activated complex in chemical reactions. *Journal of Chemical Physics, 3,* 107-115.

Eyring, H., & Polányi M. (1931). Über Einfache Gasreaktionen. *Zeitschrift für Physikalische Chemie, 12,* 279-311.

Gergely, A., Locskai, R., Szabó, P., Krójer, A., & Kristóf, T. (2016). Hydrogen sulphide corrosion of carbon and stainless steel alloys immersed in mixtures of renewable fuel sources and tested under co-processing conditions. *Hungarian Journal of Industrial Chemistry, 44,* 55-70. https://doi.org/10.1515/hjic-2016-0007

Hancock, P., & Hurst, R. C. (1974). The mechanical properties and breakdown of surface oxide films at elevated temperatures. In: Staehle RW, Fontana MG editors. Advances in corrosion science and technology. Vol. 4, Plenum, New York, pp. 1-84.

Hancsók, J., Baladincz, P., Kasza, T., Kovács, S., Tóth, C., & Varga, Z. (2011). Biogas oil production from waste lard. *Journal of Biomedical and Biotechnology ID 384184*, 9 pages.

IUPAC. Compendium of Chemical Terminology. 2nd ed. (the Gold Book). (1997). Compiled by McNaught, A. D., & Wilkinson, A. Blackwell Scientific Publications, Oxford.

John, R. C. (25–30 April, 1999). NACE International Corrosion Conference, Paper no. 073, San Antonio, Texas, 1-38.

Kim, S. J., Park, J. H., & Kim, K. Y. (2016). Effect of microstructure on sulfide scale formation and corrosion behavior of pressure vessel steel in sour environment. *Materials Characterization, 111,* 14-20. https://doi.org/10.1016/jmatchar.2015.11.007

Klass, D. L. (2004). *Biomass for renewable energy, fuels and chemicals. Encyclopedia of energy* (2st ed.). Elsevier Science, Inc.

Knothe, G., Gerpen, J. V., & Krahl, J. (2005). The biodiesel handbook, AOCS Press, Champaign, IL.

Kubicka, D., & Horacek, J. (2010). Deactivation of HDS Catalysts in Deoxygenation of Vegetable Oils. *Applied Catalysis A: General, 394*, 9-17. https://doi.org/10.1016/j.apcata.2010.10.034

Laidler, K. J., & King, M. C. (1983). Development of transition-state theory. *J Phys Chem., 87,* 2657-2664. https://doi.org/10.1021/j100238a002

Melero, J.A., Calleja, G., Garcia, A., Clavero, M., Hernandez, E. A., Miravalles, R., & Galindo, T. (2010). Hydrocracking of waste chicken fat as a cost effective feedstock for renewable fuel production: A kinetic study. *Fuel, 89*, 554-562. https://doi.org/10.1016/j.ejpe.2015.11.006

Mikulec, J., Cvengros, J., Joríkov, L., Banica, M., & Kleinová, A. (2010). Second generation diesel fuel from renewable sources. *J Cleaner Product, 18,* 917-926. DOI: 10.1016/j.jclepro.2010.01.018

Monnier, J., Tourigny, G., Douglas, W. S., Wong, A., Hogan, E. N., & Stumborg, M. (1998). Conversion of biomass feedstock to diesel fuel additive. US Patent 5 705 722.

Qu, D. R., Zheng, Y. G., Jing, H. M., Yao, Z. M., & Ke, W. (2006). High temperature naphthenic acid corrosion and sulphidic corrosion of Q235 and 5Cr1/2Mo steels in synthetic refining media. *Corrosion Science, 48,* 1960-1985. https://doi.org/10.1016/j.corsci.2005.08.016

Rémazeilles, C., Saheb, M. Neff, D., Guilminot, E., Tran, K., Bourdoiseau, J-A., Sabot, R., Jeannin, M., Matthiesen, H., Dillmann, P., & Refait, P. (2010). Micro-Raman spectra of FeS phases. *Journal of Raman Spectroscopy, 41,* 1425-1433. https://doi.org/10.1002/jrs.2717

Ren, C., Li, D., Bai, Z., & Li, T. (2005). Corrosion behavior of oil tube steel in stimulant solution with hydrogen sulfide and carbon dioxide. *Materials Chemistry and Physics, 93,* 305-309. https://doi.org/10.1016/j.matchemphys.2005.03.010

Rickard, D., & Luther, G. W. (2007). Chemistry of iron sulfides. *Chemical Reviews, 107,* 514-562. https://doi.org/10.1021/cr0503658

Saw, C. K., Lian, T., Day, S. D., & Farmer, J. C. (2006). *Report No, UCRL-TR-225388, INIS Repository, 38*, 1-30. https://doi.org/10.2172/900132

Schoonen, M. A. A., & Barnes, H. L. (1991). Reactions forming pyrite and marcasite from solution: I. Nucleation of FeS_2 below 100°C. *Geochimica et Cosmochimica Acta, 55,* 1495-1504. https://doi.org/10.1016/0016-

7037(91)90122-L

Shoesmith, D. W., Taylor, P., Bailey, M. G., & Owen, G. D. (1980). The formation of ferrous monosulfide polymorphs during the corrosion of iron by aqueous hydrogen sulfide at 21°C. *Journal of Electrochemical Society, 127,* 1007-1015. https://doi.org/10.1149/1.2129808

Slavcheva, E., Shone, B., & Turnbull, A. (1999). Review of naphthenic acid corrosion in oil refining. *Brazilian Corrosion Journal, 34,* 125-131. https://doi.org/10.1179/000705999101500761

Smith, S. N. (2015, 15–19 March) NACE International Corrosion Conference, Paper 5485, Dallas, Texas, US, pp. 1-18.

Stumborg, M., Wong, A., & Hogan, E. (1996). Hydroprocessed vegetable oils for diesel fuel improvements. *Bioresource Technology, 56,* 13-18. https://doi.org/10.1016/0960-8524(95)00181-6

Topolnitskij, P. (2007). Corrosion protection of oil production and refinery equipment. *Chemistry and Chemical Technology, 1,* 45-54.

Walendziewski, J., Stolarski, M., Łużny, R., & Klimek, B. (2009). Hydroprocesssing of Light Gas Oil—Rape Oil Mixtures. *Fuel Process Technol, 90,* 686-691. https://doi.org/10.1016/j.fuproc.2008.12.006

Wikjord, A. G., Rummery, T. E., Doern, F. E., & Owen, D. G. (1980). Corrosion and deposition during the exposure of carbon steel to hydrogen sulphide-water solutions. *Corrosion Science, 20,* 651-671. https://doi.org/10.1016/0010-938X(80)90101-8

Wu, X. Q., Jing, H. M., Zheng, Y. G., Yao, Z. M., & Ke, W. (2004). Resistance of Mo-bearing stainless steels and Mo-bearing stainless-steel coating to naphthenic acid corrosion and erosion–corrosion. *Corrosion Science, 46,* 1013-1032. https://doi.org/10.1016/S0010-938X(03)00192-6

Xie, X., & Chen, M. (2016). Suizhou Meteorite: Mineralogy and shock metamorphism. Springer geochemistry/mineralogy, Guangdong Science and Technology Press, Co. Ltd., Guangzhou, pp. 64-85.

Wang, H., & Salveson, I. (2005). A review on the mineral chemistry of the non-stoichiometric iron sulphide, Fe1-xS (0≤x≤0.125): polymorphs, phase relations and transitions, electronic and magnetic structures, *Phase Transitions, 78,* 547-567. https://doi.org/10.1080/01411590500185542

Appendix A

Materials used for the immersion type corrosion experiments

Composition of steel alloys, raw gas oil and the renewable biomass fuel sources

Table A1. Chemical composition of the carbon, low and high alloy steels in weight%

Alloys	Fe	C	Cu	Si	P	S	Mn	Cr	Ni	Mo	N	Ti
1.0425	Balance	≤0.20	≤0.30	≤0.40	≤0.025	≤0.015	1.40	≤0.30	≤0.30	≤0.08	≤0.012	≤0.03
St35.8	Balance			0.25	≤0.04	≤0.040	0.70					
1.7335	Balance	0.14	≤0.30	≤0.35	≤0.025	≤0.010	0.75	1.05		0.5		0.012
1.4541	Balance	≤0.06		≤0.75	≤0.04	≤0.015	≤2.0	18.0	10.0	-		0.70

Table A2. Characteristics of the raw gas oil

Distillation data of raw gas oil	
Boiling point of the fractions	Proportion of fractions
136.4	Initial
187.2	5
197.3	10
214.1	20
227.6	30
241.8	40

258.2	50
274.2	60
291.5	70
310.9	80
331.9	90
347.3	95
Recovery	96.7
Residue	1.5
Loss	1.8

Table A3. Characteristics of the renewable biomass fuel sources

Fuel source	Waste cooking oil	Animal waste lard
Organic acids (C1-C4, mg kg^{-1})		
Citric acid	1.90	-
Lactic acid	32.69	-
Formic acid	8.46	-
Acetic acid	64.43	94.13
Iso-butyric acid	0.00	30.83
Butyric acid	27.69	175.58
Organic acids (C8-C20, mg kg^{-1})		
Caprylic acid	1	1.5
Capric acid	-	1
Lauric acid	2	1
Myristic acid	3	11
Palmitoleatic acid	2.5	18
Heptadecanoic acid	-	3.5
γ-linoleic acid	0.6	5
Arachidic acid	-	3.5
Gondoic acid	-	7.5
Nervoic acid	-	1
Palmitic acid	100	165
Stearic acid	25	95
Oleic acid	285	310
Linoleic acid	190	65
Extractable petroleum hydrocarbons (C10-C40, mg kg^{-1})		
C36	1.15	0.30
C37	0.10	-
C38	0.15	0.24
C39	0.12	-
Iodine number (mg in 100g)	96	65
Total acid number (KOH mg g^{-1})	6	74
Molecule contents (mg kg^{-1})		
Glycerol	-	7014.05

Methanol	-	100.33
Ethanol	11.12	6.35
Water	611	1171

Appendix B

Experimental results based gravimetric measurements of the coupons

Integral and differential mass changes as function of the experimental variables

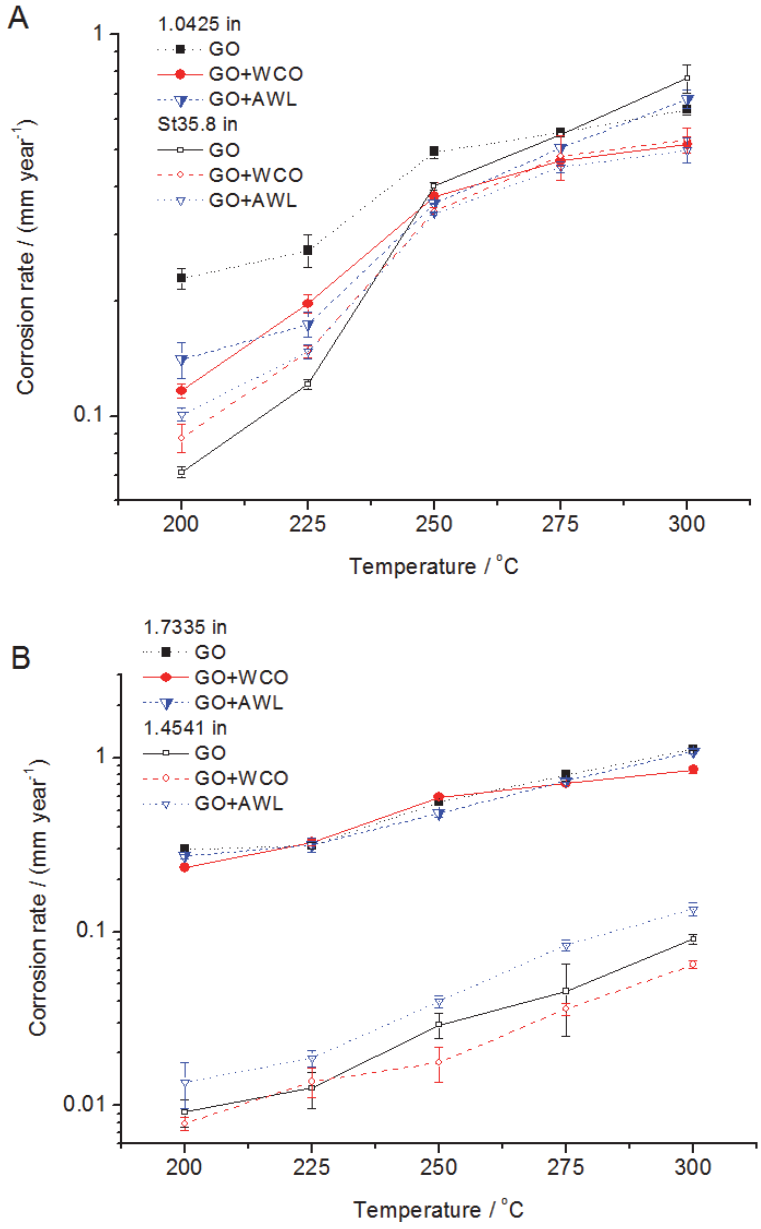

Figure B1. Integral corrosion rates expressed in mm year^{-1} obtained over a measure period of 504 hours as a function of temperature in raw gas oil (GO) and its mixture either with waste cooking oil (WCO) or animal waste lard (AWL) at an overall of 90 bar in the presence of 2 volume% hydrogen sulfide: A the 1.0425 and St35.8, B the 1.7335 and 1.4541.

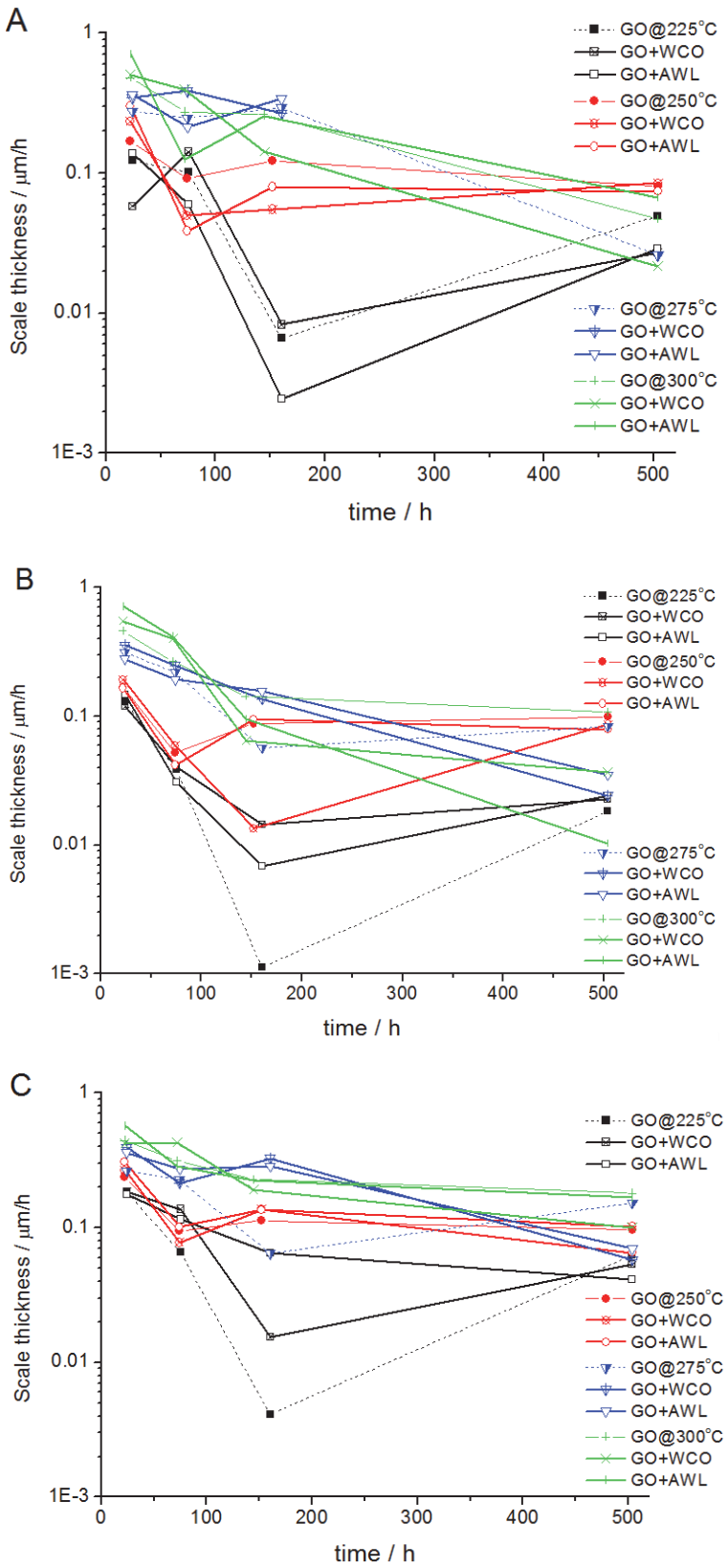
A
B
C
Scale thickness / μm/h
time / h
1
0.1
0.01
1E-3
0
100
200
300
400
500
GO@225°C
GO+WCO
GO+AWL
GO@250°C
GO+WCO
GO+AWL
GO@275°C
GO+WCO
GO+AWL
GO@300°C
GO+WCO
GO+AWL

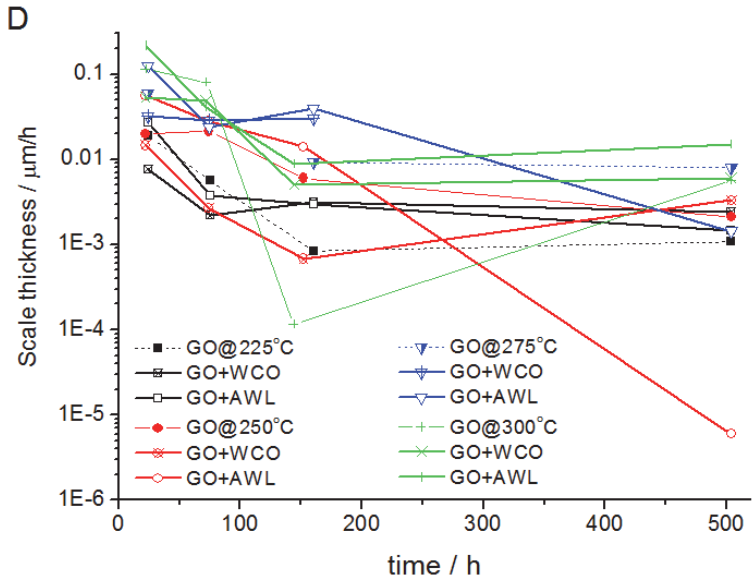

Figure B2. Hypothetical scale thicknesses, derived from differential corrosion rates, normalized to an hour over time periods based on mass change of the coupons immersed in raw gas oil (GO) and its mixture with waste cooking oil (WCO) or animal waste lard (AWL) tested at a pressure of 90 bar in the presence of 2 volume% hydrogen sulfide: A 1.0425, B St35.8, C 1.7335, D 1.4541.

Appendix C

Structure analysis result on corrosion products and surfaces of the corroded coupons

X-ray diffraction obtained from metal sulfide debris and the adherent layers

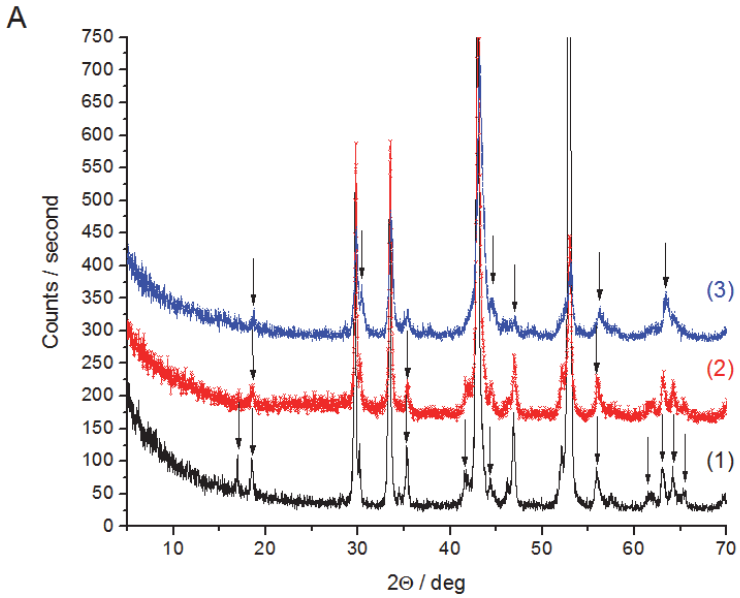

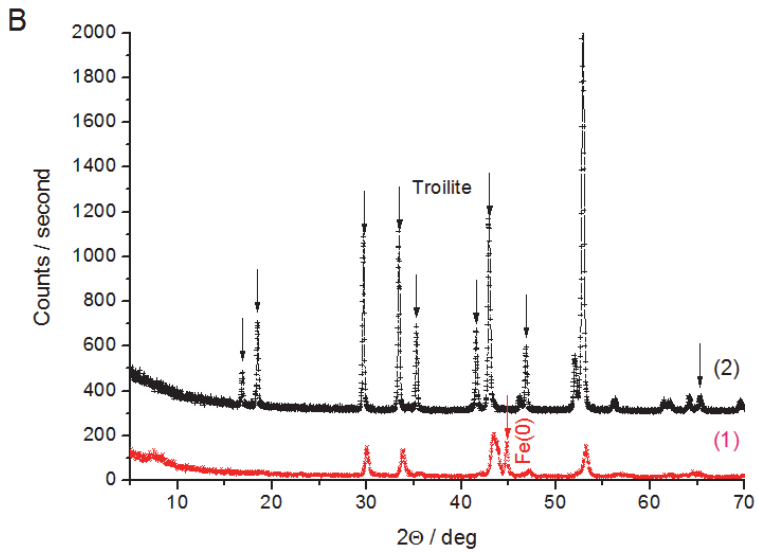

Figure C1. XRD patterns of sulfide scales: A removed from coupons of the 1.0425 carbon steel immersed in (1) raw and (2) refined gas oil tested at 250ºC, (3) the 1.7335 low alloy steel immersed in gas oil mixture with animal waste lard (10 wt.%) tested at 300ºC, all at a pressure of 90 bar for 504 hours, B sulfide scales on coupons of the St35.8 carbon steel immersed in (1) raw gas oil and its mixture with (2) animal waste lard tested at a temperature of 250ºC and a pressure of 90 bar for 168 hours